Strål säkerhets myndigheten
Swedish Radiation Safety Authority

Authors: Imre Pázsit
Victor Dykin
Anders Jonsson
Christophe Demazière

Research

2010:22

Research and Development Program in Reactor Diagnostics and Monitoring with Neutron Noise Methods, Stage 16

Report number: 2010:22 ISSN: 2000-0456
Available at www.stralsakerhetsmyndigheten.se

Title: Research and Development Program in Reactor Diagnostics and Monitoring with Neutron Noise Methods, Stage 16
Report number: 2010:22
Author: Imre Pázsit, Victor Dykin, Anders Jonsson and Christophe Demazière
Chalmers University of Technology, Department of Nuclear Engineering, SE-412 96 Göteborg
Date: December 2010

This report concerns a study which has been conducted for the Swedish Radiation Safety Authority, SSM. The conclusions and viewpoints presented in the report are those of the authors and do not necessarily coincide with those of the SSM

SSM Perspective

Background

This report constitutes Stage 16 of a long-term research and development program concerning the development of diagnostics and monitoring methods for nuclear reactors.
Results up to Stage 15 were reported in SKI and SSM reports, as listed below and in the Summary. The results have also been published in international journals and have been included in both licentiate- and doctor's degrees.

Objectives of the project

The objective of the research program is to contribute to the strategic research goal of competence and research capacity by building up competence within the Department of Nuclear Engineering at Chalmers University of Technology regarding reactor physics, reactor dynamics and noise diagnostics. The purpose is also to contribute to the research goal of giving a basis for SSM's supervision by developing methods for identification and localization of perturbations in reactor cores.

Results

The program executed in Stage 16 consists of the following three parts:

- An overview of the present status of experience with BWR stability;
- An investigation of the significance of the properties of the noise source for BWR instability;
- Study of the dynamics of molten salt systems: construction of the adjoint and calculating the space dependent noise induced by propagating perturbations in the fuel;
- A specific study of some novel methods of analysis of non-linear and non-stationay processes.

Project information

Responsible at SSM has been Ninos Garis.
SSM reference: SSM 2009/2093
Previous SKI reports: 95:14 (1995), 96:50 (1996), 97:31 (1997), 98:25 (1998), 99:33 (1999), 00:28 (2000), 01:27 (2001), 2003:08 (2003), 2003:30 (2003), 2004:57 (2004), 2006:34 (2006), 2008:39 (2008),
Previous SSM reports: 2009:38 (2009)

Contents

Contents 1
Summary 3
Sammanfattning 7
1 An overview of the present status of experience with BWR stability 10
1.1 Introduction 10
1.2 Determination of the Decay Ratio in BWRs 10
1.3 Stability indicator 12
1.4 Stability mechanism of a BWR 12
1.5 Types of BWR instabilities 14
1.6 Combined types of oscillations 18
2 An investigation of the significance of the properties of the noise source for BWR instability 23
2.1 Introduction 23
2.2 Calculations for a white noise driving force 24
2.3 The reactivity effect of propagating perturbations: a non-white driving force. 24
2.4 Calculations for the non-white driving force. 26
2.5 Analysis of the results 28
2.6 Conclusions 32
3 Study of the dynamics of molten salt systems: construction of the adjoint and calculating the space dependent noise induced by propagating perturbations in the fuel 34
3.1 Introduction 34
3.2 The adjoint function 35
3.3 The Greens function 37
3.4 Propagating perturbations 41
4 A specific study of the novel methods of analysis of non-linear and non-stationary processes 46
4.1 Introduction 46
4.2 Principles 46
4.3 Peak-to-peak time interval analysis of BWR in-core neutron noise signals 47
4.4 Principal Component Analysis and Singular Value Decomposition 52
4.5 Conclusions 57
Plans for the continuation 58
Acknowledgement 58
References 58

Summary

This report gives an account of the work performed by the Department of Nuclear Engineering, Chalmers University of Technology, in the frame of a research contract with the Swedish Radiation Safety Authority (SSM), contract No. SSM 2009/2093. The present report is based on work performed by Imre Pázsit, Victor Dykin, Anders Jonsson and Christophe Demazière, with Imre Pázsit being the project leader.

This report describes the results obtained during Stage 16 of a long-term research and development program concerning the development of diagnostics and monitoring methods for nuclear reactors. The long-term goals are elaborated in more detail in e.g. the Final Reports of Stage 1 and 2 (SKI Report 95:14 and 96:50, Pázsit et al. 1995, 1996). Results up to Stage 15 were reported in (Pázsit et al. 1995, 1996, 1997, 1998, 1999, 2000, 2001, 2003a, 2003b; Demazière et al, 2004; Sunde et al, 2006; Pázsit et al. 2008, 2009). A brief proposal for the continuation of this program in Stage 17 is also given at the end of the report.

The program executed in Stage 16 consists of four parts as follows:

- An overview of the present status of experience with BWR stability;
- An investigation of the significance of the properties of the noise source for BWR instability;
- Study of the dynamics of molten salt systems: construction of the adjoint and calculating the space dependent noise induced by propagating perturbations in the fuel;
- A specific study of some novel methods of analysis of non-linear and non-stationary processes.

The work performed in each part is summarized below.

1. An overview of the present status of experience with BWR stability

This section gives an overview of the main trends in BWR stability analysis and monitoring for the past decade. The major line of development in this period has been the recognition that different types of neutronic and thermal hydraulic oscillations may occur (global, regional and local or channel-type), with different generation mechanisms, impact on core safety, and monitoring tools and needs. In particular, when any two of these types can occur simultaneously, it is important to separate the different components, otherwise the margin to instability can be misjudged severely. Any procedure aiming at stability monitoring should be able to detect the presence of simultaneous oscillations, as well as to classify their type and stability properties separately. In this respect global and regional type instabilities are a larger potential operational problem than local oscillations, because their amplitude can grow unbounded. Local oscillations are purely thermal hydraulics driven, and it is not so much the stability properties than the localisation which is of concern.

This section starts with a description of the three main oscillation types and their properties. The concept of the most commonly used stability parameter, the decay ratio,

is described. The properties of simultaneous oscillations and the resulting apparent decay ratio obtained without separation of the components are discussed. The methods elaborated to separate the global and regional oscillations are described in detail. The noise simulator, developed at the department, is used to reconstruct some of the observed properties, such as the space dependence of the decay ratio in case of simultaneous oscillations of two different types. The localisation of a local channel-type instability is also described and its concrete application to the case of the Forsmark local instability is demonstrated.

2. An investigation of the significance of the properties of the noise source for BWR instability

In simple models used to interpret the stability properties of boiling water reactors it is assumed that the power or flux oscillations in the core can be described as the response of a damped linear oscillator, driven by a white noise driving force. Such a model proves useful in understanding the path to instability, especially the interplay of several different oscillation modes (global, regional, local). In the model it is assumed that the stability properties, extracted from the measured oscillations, are determined purely by the system transfer properties, due to the fact that the driving force has a spectrum which is constant in frequency.

However, from other studies of BWR in-core noise, it is known that the reactivity perturbation corresponding to the propagating character of two-phase flow has a characteristic autospectrum which shows a periodic peak and sink structure, i.e. deviates markedly from white noise. In that case, the frequency properties, or the autocorrelation function of the measured detector signals, are influenced not only by the system transfer properties, but also by those of the driving force. Estimating the decay ratio with the assumption of white driving force can lead to erroneous results.

The influence of the "coloured" character of the driving force, as represented by the reactivity perturbation of propagating density fluctuations of the two-phase flow, on the estimation of the decay ratio is investigated. The autocorrelation function of the system response with such a coloured driving force is calculated analytically. Cases when the driving force has a peak or a sink at the system resonance frequency are investigated quantitatively. The results show that in the case of propagating perturbations the structure of the driving force is relatively smooth at the system resonance, and no significant error is made in the estimation of the decay ratio assuming a white noise driving force.

3. Study of the dynamics of molten salt systems: construction of the adjoint and calculating the space dependent noise induced by propagating perturbations in the fuel

In previous reports, starting with Stage 13, a simple one-dimensional model with propagating fuel properties was set up and studied as a model of a molten salt reactor. First the solution of the static eigenvalue equation was given first by expansions into eigenfunctions of a corresponding traditional reactor. The neutron noise, induced by propagating perturbations, was calculated in the point kinetic approximation, by using a simplified empirical model of the zero reactor transfer function $G_0(\omega)$, suggested in the

literature. It was also noticed that the derivation of the point kinetic approximation with the flux factorisation technique is hindered by the fact that the one-group diffusion equations for a reactor with moving fuel are not self-adjoint.

In Stage 15, the solution of the space-dependent noise problem was started with the calculation of the Green's function of the problem. The space-dependent problem was solved for the case of infinite fuel velocity, with a new technique which separates out a singular and a non-singular term in the solution, similarly to the method of eliminating the uncollided flux in transport problems.

In the present Stage, first the adjoint equations of the one-group diffusion theory are derived for reactors with moving fuel. The adjoint property of the suggested form is proven both for the differential form of the coupled neutron-precursor equations, and for the integro-differential form, obtained after eliminating the delayed neutron precursors. Then the Green's function of the reactor is calculated for finite fuel velocities, with the employment of a method, suggested in the previous Stage for the solution for infinite fuel velocities. The space and frequency dependence of the Green's function is investigated. Finally, the space-dependent noise, induced by propagating perturbations, are calculated and discussed. It is shown that with increasing fuel velocity, the behaviour of a given system at a given frequency tends to be more and more point kinetic, in accordance with the results for infinite fuel velocity, found in the previous Stage.

4. A specific study of some novel methods of analysis of non-linear and non-stationary processes

New methods have been developed lately which are particularly useful to analyse non-stationary processes in order to make a diagnosis of the state of the system. Some of the development has been achieved primarily in biology and medicine, for the analysis of ECG (heart beat) and EEG (brain activity) signals and to detect beginning and developed diseases. Some of these methods were transferred even to the diagnostics of process signals in power plants. The purpose of this pilot study is to start exploring the application of such methods in reactor diagnostics.

One such method refers to the analysis of quasi-periodic signals, such as human ECG signals. Instead of analysing the raw signal, a secondary time series is derived from the original signal, which consists of the sequence of beat-to-beat (also called "interbeat") time intervals. This derived sequence is apparently random, but it contains a substantial information on the status of the system. This information can be extracted either from the topology of the three dimensional vectors, formed from triplets of consecutive values of the interbeat intervals, of from the fractal dimension of the data series, or by some other intelligent identification method.

In this Stage the method of peak-to-peak interval analysis is tested on measurements of BWR instability. The time series represented by the peak-to-peak time intervals of the signal variation around the instability frequency 0.5 Hz is analysed. First a method was developed for the extraction of the peak-to-peak series, then the topology of the three-dimensional vectors, formed from data triplets, was investigated. A different behaviour was found for the cases of a stable and an unstable state of the core, although the information content was rather obvious. Some new algorithmic identification methods,

such as Principal Component Analysis (PCA) and Singular Value Decomposition (SVD), were also tested on the data vectors, but these yielded no further information. These studies will be continued with e.g. using higher dimensional data sets, to explore their potential in BWR stability analysis.

Sammanfattning

Denna rapport redovisar det arbete som utförts inom ramen för ett forskningskontrakt mellan Avdelningen för Nukleär Teknik, Chalmers tekniska högskola, och Strålsäkerhetsmyndigheten (SSM), kontrakt Nr. SSM 2009/2093. Rapporten är baserad på arbetsinsatser av Imre Pázsit, Victor Dykin, Anders Jonsson och Christophe Demazière, med Imre Pázsit som projektledare.

Rapporten beskriver de resultat som erhållits i etapp 16 av ett långsiktigt forsknings- och utvecklingsprogram angående utveckling av diagnostik och övervakningsmetoder för kärnkraftsreaktorer. De långsiktiga målen har utarbetats noggrannare i slutrapporterna för etapp 1 och 2 (SKI Rapport 95:14 och 96:50, Pázsit et al. 1995, 1996). Uppnådda resultat fram till och med etapp 15 har redovisats i referenserna (Pázsit et al. 1995, 1996, 1997, 1998, 1999, 2000, 2001, 2003a, 2003b; Demazière et al, 2004; Sunde et al, 2006; och Pázsit et al. 2008, 2009). Ett kortfattat förslag till fortsättning av programmet i etapp 17 redovisas i slutet av rapporten.

Det utförda forskningsarbetet i etapp 16 består av följande fyra olika delar.

- Sammanställning av kunskapsläget för BWR-instabilitet;
- Undersökning av betydelsen av bruskällan i samband med BWR-instabilitet;
- Fortsatta studier av neutronkinetik, dynamik och neutronbrus i reaktorer med flytande bränsle (MSR);
- Undersökning och tillämpning av "intelligent computing" metoder.

Arbetet med varje del sammanfattas nedan.

1. Sammanställning av kunskapsläget för BWR-instabilitet

Denna del ger en överblick av de huvudsakliga trenderna i stabilitetsanalys och övervakning av BWR-reaktorer under det senaste decenniet. Den huvudsakliga utvecklingen under denna period har varit insikten om att olika typer av neutron- och termohydrauliska oscillationer kan förekomma (globala, regionala och lokala eller kanaltyp). Dessa genereras av olika mekanismer och har olika inverkan på härdsäkerhet, övervakningsinstrument och övervakningsbehov. I synnerhet när två av dessa typer kan uppträda samtidigt är det viktigt att separera de olika komponenterna för att inte marginalen till instabilitet väsentligt ska missbedömas. En metod för stabilitetsövervakning måste kunna upptäcka närvaron av samtidiga oscillationer samt klassificera dess typ och stabilitetsegenskaper var för sig. I detta avseende utgör globala och regionala instabiliteter troligen ett större driftsproblem än lokala oscillationer, eftersom deras amplitud kan växa obegränsat. Lokala oscillationer har enbart termohydrauliska orsaker och det handlar i detta fall inte så mycket om stabilitetsegenskaper som att lokalisera oscillationen.

Avsnittet inleds med en beskrivning av de tre huvudsakliga oscillationstyperna och deras egenskaper. Begreppet dämpkvot, som är den mest använda stabilitetsparametern, beskrivs. Egenskaperna hos samtidiga oscillationer och den resulterande faktiska dämpkvot, som erhållits utan att separera komponenterna, diskuteras. Metoderna, som utarbe-

tats för att separera globala och regionala oscillationer, beskrivs i detalj. Brussimulatorn, som utvecklats vid avdelningen, används för att rekonstruera några av de observerade egenskaperna såsom rumsberoendet hos dämpkvoten när det finns samtidiga oscillationer av två olika slag. Hur en lokal kanaltyp-instabilitet lokaliseras beskrivs också och dess tillämning på fallet av den lokala instabiliteten i Forsmark demonstreras.

2. Undersökning av betydelsen av bruskällan i samband med BWR-instabilitet

I de enkla modeller, som använts för att tolka stabilitetsegenskaperna i kokvattenreaktorer, antas att effekt- eller flödesoscillationerna i härden kan beskrivas som svaret på en dämpad linjär oscillator som drivs av vitt brus. En sådan modell visar sig användbar för förståelsen av hur instabilitet uppkommer, särskilt samspelet mellan flera olika oscillationsmoder (globala, regionala, lokala). I modellen antas att stabilitetsegenskaperna, som konstruerats från uppmätta oscillationer, enbart bestäms av systemets överföringsegenskaper p.g.a. det faktum att drivkraften har ett spektrum med konstant frekvens.

Från andra studier av härdbrus i BWR är det emellertid känt att de reaktivitetsstörningar, som svarar mot tvåfasflödets spridningsegenskap, har ett karaktäristiskt spektrum med en periodisk topp- och dalstruktur, dvs. avviker markant från vitt brus. I detta fall påverkas frekvensegenskaperna, eller autokorrelationsfunktionen till de uppmätta detektorsignalerna, inte enbart av systemets överföringsegenskaper, utan även av drivkraftens egenskaper. Beräkning av dämpkvoten med antagande om vitt brus som drivkraft kan leda till felaktiga resultat.

Hur den ”färgade” egenskapen hos drivkraften, representerad av reaktivitetsstörningar i tvåfasflödets icke-stationära täthetsfluktuationer, påverkar beräkningen av dämpkvoten undersöks. Autokorrelationsfunktionen till systemets reaktion på en sådan färgad drivkraft beräknas analytiskt. Fall där drivkraften har en topp eller sänka vid systemets resonansfrekvens undersöks kvantitativt. Resultaten visar att när vi har icke-stationära störningar så blir drivkraftens struktur relativt mjuk vid systemets resonans och att anta att vitt brus är drivkraften innebär inget signifikant fel i beräkningen av dämpkvoten.

3. Fortsatta studier av neutronkinetik, dynamik och neutronbrus i reaktorer med flytande bränsle

I tidigare rapporter, med början på etapp 13, konstruerades och studerades en enkel endimensionell modell av en smältsaltereaktor där bränsleegenskaperna förflyttas. Lösningen till den statiska egenvärdesekvationen gavs först som utvecklingar i egenfunktioner till en motsvarande traditionell reaktor. Neutronbruset, som härrör från icke-stationära störningar, beräknades med den punktkinetiska approximationen genom att använda en förenklad empirisk modell av överföringsfunktionen $G_0(\omega)$ för en nolleffektreaktor, som föreslagits i litteraturen. Det observerades också att härledningen av den punktkinetiska approximationen med faktoriseringsteknik för flödet förhindras av att engruppsdiffusionsekvationen för en reaktor med rörligt bränsle inte är självadjungerad.

I etapp 15 påbörjades lösningen av det rumsberoende brusproblemet med beräkningen av Greens funktion för problemet. Det rumsberoende problemet löstes för fallet med

oändlig bränslehastighet med en ny teknik som separerar ut en singulär och en icke-singulär term i lösningen på samma sätt som när det okolliderade flödet i transport-problem elimineras.

I denna etapp deriveras först den adjungerade ekvationen för engruppsdiffusionsteori för reaktorer med rörligt bränsle. Den adjungerade egenskapen av den föreslagna formen bevisas både för den differentiala formen av de kopplade neutron-föregångar-ekvationerna och för integro-differentialformen, som erhållits efter eliminering av de fördröjda neutronföregångarna. Sedan beräknas reaktorns Greens-funktion för ändliga bränslehastigheter med en metod som föreslagits i den tidigare etappen för lösning vid oändlig bränslehastighet. Rums- och frekvensberoendet hos Greens funktion undersöks. Slutligen beräknas och diskuteras det rumsberoende brus, som orsakats av icke-stationära störningar. Det visas att med ökande bränslehastighet blir beteendet hos ett givet system vid en given frekvens mer och mer punktkinetiskt, i överensstämmelse med de resultat för oändlig bränslehastighet, som fastställts i den tidigare etappen.

4. Undersökning och tillämpning av “intelligent computing” metoder

På sista tiden har nya metoder, speciellt användbara för att analysera icke-stationära processer, utvecklats för att diagnosticera tillståndet i ett system. Viss utveckling har erhållits primärt inom biologi och medicin för analys av signaler från ECG (hjärtslag) och EEG (hjärnaktivitet) och för att upptäcka begynnande och utvecklade sjukdomar. Några av dessa metoder har överförts till diagnos av processignaler i kärnkraftverk. Målsättningen med denna pilotstudie är att börja undersöka hur sådana metoder kan appliceras inom reaktordiagnostik.

En sådan metod hänför sig till analysen av kvasiperiodiska signaler såsom mänskliga ECG-signaler. Istället för att analysera den obearbetade signalen tas en sekundär tidsserie, som består av sekvensen av tidsintervall mellan hjärtslagen, fram ur den ursprungliga signalen. Denna härledda sekvens är uppenbart slumpmässig, men den innehåller väsentlig information om systemets tillstånd. Sådan information kan extraheras antingen från topologin hos de tredimensionella vektorer, som formas av tripletter av på varandra följande värden av hjärtslagsintervall, från dataseriens fraktala dimension eller genom någon annan intelligent identifieringsmetod.

I denna etapp testas metoden med intervallanalys topp till topp på mätningar av instabiliteter i BWR. Tidsserierna, som representeras av tidsintervallen topp till topp hos signalvariationen runt instabilitetsfrekvensen 0.5 Hz, analyseras. Först utvecklades en metod för att extrahera topp till topp-serien. Sedan undersöktes topologin hos de, av datatripletter bildade, tredimensionella vektorerna Ett annorlunda beteende hittades för fallen med ett stabilt och ett instabilt tillstånd hos härden, fast informationsinnehållet var ganska uppenbart. Några nya algoritmmetoder för identifikation, såsom ”Principal Component Analysis” (PCA) och ”Singular Value Decomposition” (SVD), testades också på datavektorerna, men dessa gav ingen ytterligare information. Dessa studier ska fortsätta med att t.ex. undersöka vilka möjligheter dataset av högre dimension har för att analysera BWR-stabilitet.

1 An overview of the present status of experience with BWR stability

1.1 Introduction

This chapter gives an overview of the status of characterisation of the stability of BWRs and methods of quantifying and monitoring margins to instability. The status of the methods and concepts applied is described, together with a summary of the main concepts and the current development trends.

The chapter is based on material published in a lecture note used at a Workshop at ICTP Trieste in 2008 (Demazière and Pázsit 2008) as well as a chapter in a current 5-volume Handbook of Nuclear Engineering by Springer (Pázsit and Demazière 2010).

1.2 Determination of the Decay Ratio in BWRs

Instability of BWRs, which is manifested by self-sustained power oscillations in the core, has been observed at the very early days of reactor operation, and the possibility of BWR instability was predicted by Thie (1959). Such instabilities are usually encountered during start-up conditions, i.e. at reduced core flow and relatively high power level. Calculations are thus performed via adequate coupled neutronic/thermal-hydraulic codes to verify under which conditions the reactor becomes unstable. This defines an exclusion zone, i.e. a set of operating conditions on the power-flow map, which the reactor operator should always avoid. During the start-up tests of the reactor, measurements of the in-core neutron noise are usually performed. The goal of these measurements is to verify that there is a good agreement with the calculations.

Monitoring the stability with measurements, as well as determining the margins to instability requires the existence of a reliable quantitative stability indicator. Such a parameter should be an integral, global parameter of the core, similar to the reactivity. However, as will be clear from the discussion below, the situation is more involved because, unlike with the definition of the reactivity, the stability cannot be characterized only with quantities belonging to the fundamental eigenvalue and fundamental eigenmode. Also, there are several possibilities for choosing a stability parameter, out of which we will only discuss the most common one, the Decay Ratio.

BWR instability is an intriguing subject far from being fully understood, and accordingly it has a vast literature (for a review see D'Auria et al., 1997). To illus-trate the point we list here a number of references, still far from being complete, to give a flavor of the diversity and vibrant character of the research in the field: Hagen et al. (1994); Takeuchi (1994); Hennig (1999); Hotta et al. (1997); Oguma (1997); Karlsson and Pázsit (1999); Miro et al. (2000); Ginestar et al. (2002,2006); Munoz-Cobo et al. (2004) Demazière and Pázsit (2005); Zinzani et al. (2008).

.

Although in many cases the stability of BWRs can be investigated by small linear fluctuations around a stationary state of the system, in principle the dynamics of a BWR is a strongly non-linear system. Despite of this, in this section we will focus on stability

analysis in the linear regime, because the methods used in practice are based on techniques of linear analysis. However, characterizing and understanding non-linear aspects and developing non-linear diagnostics methods are also under development. These follow two different lines. One is setting up simple non-linear models in which certain aspects of the non-linear behaviour, such as bifurcations, limit cycles etc. can be studied with analytical or simple numerical methods (Cacuci 1983; March-Leuba et al., 1983, 1984a, 1984b, 1986a, 1986b; Cacuci et al., 1986; Konno et al., 1999). The content of these works will not be described here, partly due to limitation of space, and partly because they mostly aim for understanding but not for practical methods of diagnostics and monitoring

The other development line is based on the recognition that non-linear models very seldom have analytical solutions, hence the study of such systems must rely on numerical treatment of large number of coupled non-linear partial differential equations describing the system. So-called advanced system codes exist which describe the static and dynamic behaviour of the system with high accuracy. However, such codes are only practical for calculating particular singular cases but not a large series of calculations due to the large computational load. Besides, due to the large number of input-output variables needed to achieve high fidelity of the calculations, such system codes lend very little, or none, insight and understanding to identify important features in the development and characterisation of instability. Hence, for studying non-linear phenomena with insight, calculational models are used which keep the full non-linear relationships between the important parameters, but simplify the geometry of the arrangement by replacing the core with a small number, so far one or two, thermal hydraulic channels and corresponding lumped core regions. Such models are commonly used Reduced Order Models (ROMs) (March-Leuba, 1984b; Lahey 1992; Karve 1998; Dockhane 2004; Lange 2009).

Our department has therefore become involved in the development of a ROM which represents an extension compared to previous work in that it contains four thermal hydraulic channels, whereas former models used only one or at most two channels. The full description of this work can be found in Dykin, Demazière, 2010a; Dykin 2010b. Here below we just summarize the work done, which thus will give an outline of the frontline of research in this area.

As as first step, a reduction procedure which allows one to transform 3D space-time dependent two-group diffusion equations into the point kinetic time-dependent equations is performed (Bell, Glasstone, 1970; Lamarsh 2002). Only the first three modes, namely the fundamental, first and second azimuthal modes are taken into consideration. As a second step, the general energy balance equations for the fuel rod heat conductivity are reduced to ordinary differential equations, assuming the two piecewise quadratic spatial approximation for the fuel pellet temperature and applying the variational principle approach (Karve 1998). As a last step, the reduced ordinary differential equations (ODEs) are derived for the two coolant phase regions (single and two phase regions) (Karve 1998). One starts from the general flow cross-section averaged balance equations (Todreas, Kazimi, 1990), assuming the proper spatial quadratic distribution for the enthalpy and equality, respectively, and applies the variational method to approach the final goal. Further, the corresponding ODE for the inlet coolant velocity is demonstrated, based on the pressure balance equation where a simple downcomer model, as a unheated channel, is introduced as well (Dockhane 2004,

Lange, 2009). In order to properly simulate azimuthal modes, one introduces a four heated channel model (Dykin, Demazière, 2010a; Dykin 2010b). An adjusting procedure is used for the steady-state ROM parameters, needed to reproduce the correct operational conditions (Lange 2009). This model is capable to investigate concrete instability events, such as the Forsmark-1 channel instability event, with ROM analysis. This work is on-going and results will be reported in the continuation.

1.3 Stability indicator

The most commonly used stability indicator is the so-called Decay Ratio (DR). One of the basic assumptions in the use of the DR is that the system dynamics can be modelled by a second-order oscillator, i.e. any fluctuation related to BWR instabilities obeys the following equation

$$\delta\ddot{\Psi}(t) + 2\xi\omega_0\delta\dot{\Psi}(t) + \omega_0^2\delta\Psi(t) = f(t) \tag{1}$$

where $f(t)$ represents the driving force of the oscillation, usually assumed to be a white noise, ω_0 is the resonance frequency, and ξ characterizes the damping of the system. The general solution to this equation is given by:

$$\delta\Psi(t) = A\exp(-\xi\omega_0)\cos\left[\omega_0\ \sqrt{1-\xi^2}\ \ t+\varphi\right] \tag{2}$$

The DR gives a measurement of the damping of the system and is defined as the ratio between two consecutive maxima of the signal form given above and found to be given, in the case of a second-order system, as

$$DR = \exp\left(\frac{-2\pi\xi}{\sqrt{1-\chi\zeta^2}}\right) \tag{3}$$

In practice, it is not the signal itself, but the Auto-Correlation Function (ACF) of the normalized neutron density, or alternatively the Impulse Response Function (IRF) as calculated by using an Autoregressive Moving-Average (ARMA) or an Autoregressive model (AR), are used. In case of a white noise driving force, these functions all have the same oscillatory and decaying properties as the determines-tic solution (2). Hence the DR is usually determined from the ratio between two consecutive maxima Ai and Ai+1 of any of these two functions. The ACF and IRF obtained in the case of a second-order system are represented in Fig. 1. The DR gives therefore a measure of the inherent damping properties of the sys-tem. Using each detector separately allows estimating the Decay Ratio (DR) ac-cording to the following standard method (for a review, see D'Auria, et al., 1997)

$$DR = \frac{A_{i+1}}{A_i}, \qquad \forall i \tag{4}$$

If the dynamics of the system does not correspond to a pure second-order system, the above formula gives different results depending on which consecutive peaks of the ACF or of the IRF one considers.

1.4 Stability mechanism of a BWR

Nuclear reactors must be designed such that they have a negative feedback mechanism, i.e. any perturbation leading to off-normal conditions should be counteracted by some

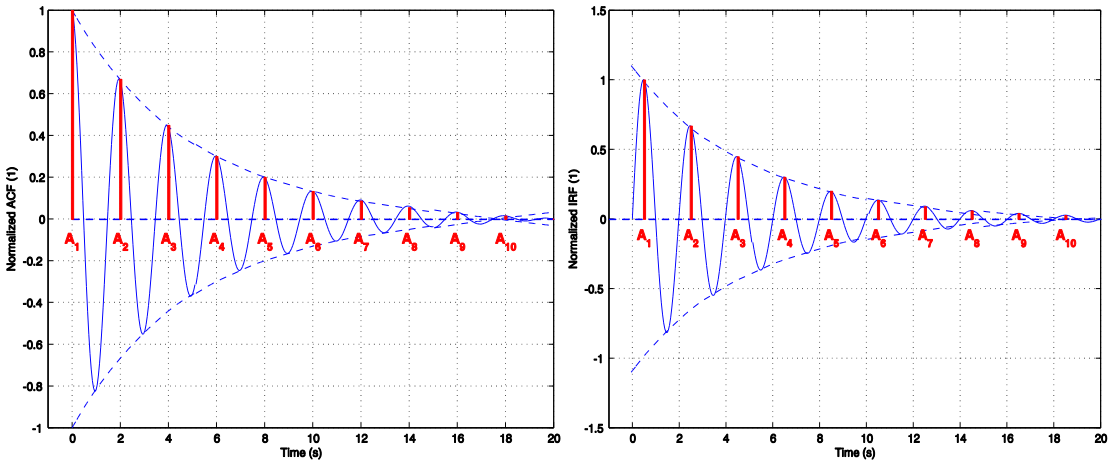

Fig. 1. ACF and IRF of a second-order system (on the left and right hand-sides, respectively)

feedback, which thus brings the system back to steady-state conditions. Instabilities can arise from the fact that in a dynamic case, such feedback mechanisms act with some time delay. If the feedback was always exactly counteracting the original perturbation without time delay, the phase shift between the perturbation and the feedback should be -180 deg (i.e. out-of-phase). Nevertheless, in most cases, the phase shift differs from -180 deg. As a result, the feedback reinforces the original perturbation instead of damping it during some parts of a period.

Several physical mechanisms are responsible for the feedback in a BWR. The ones that might give rise to instabilities are the channel thermal-hydraulics (Density Wave Oscillation, DWO) and the void-reactivity feedback. In the following, these two mechanisms are detailed. How these processes are driving instabilities will be explained in the next subsection.

A DWO corresponds to a change of the density of the coolant within one or several fuel assemblies. For illustration purposes, one can consider a perturbation induced by an inlet flow perturbation to a fuel assembly. Such an inlet perturbation will create a modification of the single-phase pressure drop in the single-phase region of the heated channel. This perturbation will travel upwards with the flow and will itself generate a modification of the two-phase pressure drop in the two-phase region of the heated channel.

The void-reactivity feedback comes from the fact that any modification of the density of the coolant affects the neutron moderation. More specifically, any decrease in the moderator density leads to a worsening of the neutron moderation. Such an effect is typically represented by the void coefficient of reactivity, i.e.

$$\alpha_{\nu} = \frac{\partial \rho}{\partial \nu} \tag{5}$$

where $\delta\rho$ represents the change of reactivity of the system due to a change $\partial\nu$ of the void fraction, with the void fraction being defined as the relative volume of vapour

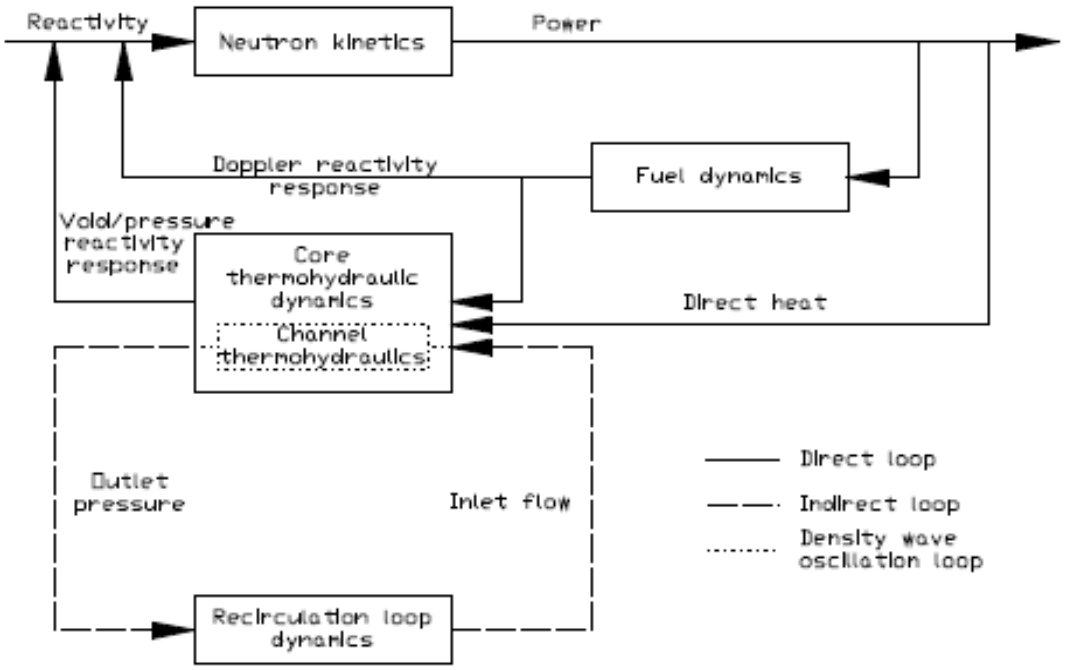

Fig. 2. Stability mechanism of a BWR

contained in a specific volume. Such a reactivity coefficient is strongly negative for BWRs.

Any perturbation of the reactivity of the system will lead to a perturbation of the reactor power and of the produced heat, which in turn will create a modification of the fuel temperature and of the void fraction. Because of the Doppler fuel temperature effect and of the void-reactivity feedback, such perturbations will affect the reactivity of the system. This feedback loop is called the direct loop. Further, a so-called recirculation loop is connected to the downcomer of a BWR. Such a loop has its own dynamical properties. As a consequence, any perturbation of the core outlet pressure will give rise to perturbation of the core inlet flow via the recirculation loop dynamics. Such a feedback loop is called the indirect loop. Finally, each fuel channel has its own dynamical properties from a thermal-hydraulic point-of-view. Any perturbation to the channel thermal-hydraulics will give rise to DWOs, and this corresponds to the so-called DWO loop in the stability mechanism of a BWR.

1.5 Types of BWR instabilities

Three types of instabilities are usually encountered in forced-circulation BWRs: pure DWOs or local oscillations, global (or in-phase) oscillations, and re-gional (or out-of-phase) oscillations. Whereas the global and regional oscillations also involve DWOs in the core, the instabilities are driven by the void-reactivity feedback, as will be explained in the following. The stability mechanism of a BWR is shown in Fig. 2.

Instabilities due to pure DWOs might occur when the boundary conditions of the heated channel(s) are imposed, as is the case for the pressure drop between the inlet and outlet

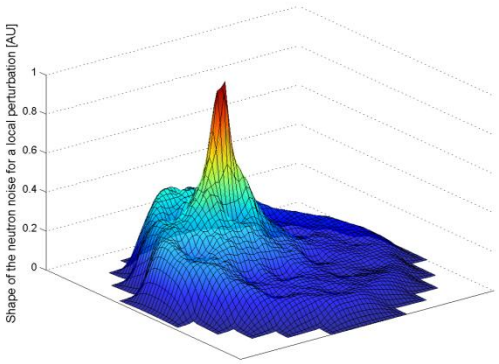

Fig. 3. Space-dependence of the neutron noise induced by a local oscillation as calculated by the neutron noise simulator

of the channels. Such instabilities are usually referred to as pure DWO or local oscillations. Due to this imposed boundary condition, the two-phase pressure drop in the perturbed fuel channel will create a feedback pressure perturbation of the opposite sign in the single-phase region, either reinforcing or damping the initial perturbation (see Yadigaroglu and Bergles, 1972) This pressure drop oscillation can also be translated into a perturbation of the coolant density (explaining the name of DWO for this kind of perturbation). The typical frequency at which such oscillations are encountered is around 0.5 Hz, which is related to the transit time of perturbations from the inlet to the outlet of the fuel assemblies. This type of oscillation typically occurs when a fuel assembly is unseated, i.e. does not sit properly on the lower fuel tie plate of the core. Since each fuel assembly in a BWR is contained in a fuel box, the fuel channels are independent from each other. Therefore, in case of an unseated fuel assembly, some of the coolant bypasses the fuel channel. This reduces the single-phase pressure drop at the inlet of the channel, and destabilizes it. Radially, this perturbation is equivalent to a local noise source, or a so-called absorber of variable strength-type of noise source and can be modelled by the neutron noise simulator developed at the Department of Nuclear Engineering, Chalmers (Demazière, 2004). An example of the results of such a modelling is presented in Fig. 3. The induced neutron noise has thus its largest amplitude at the position of the noise source, and has a fast spatial decay away from it.

Instabilities due to the void-reactivity feedback may also occur in a BWR. The mechanism driving this kind of oscillation is mainly the time-delay between a given power perturbation and the corresponding reactivity response due to the void/pressure coefficient. In some cases, the initial perturbation can be reinforced by the void/pressure feedback if the phase of this delayed response coincides with the phase of the power perturbation. It has to be emphasized that these instabilities also involve density waves through the core, but such waves alone are not responsible for the oscillations. Two types of instabilities involving such a coupling between the neutron kinetics and the thermal-hydraulics are usually encountered: in-phase (or global) oscillations, and out-of-phase (or regional) oscillations. In order to better understand the spatial dependence of such oscillations, the neutron flux can be expanded on the eigenfunctions of the system as:

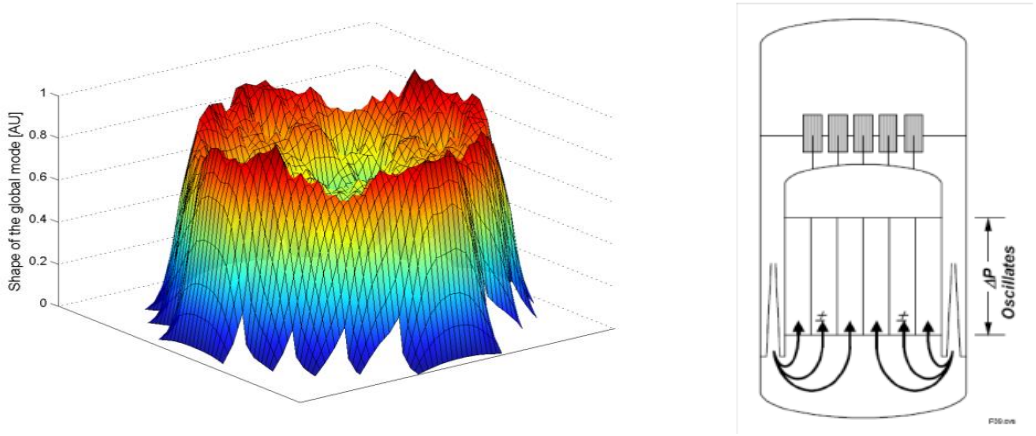

Fig. 4. Space-dependence of the neutron noise induced by a global oscillation as calculated by the neutron noise simulator (on the left hand-side) and conceptual illustration of the in-phase behavior of the flow and power oscillations (on the right hand-side) (from Siralkar, 2005)

$$\phi(\boldsymbol{r},t) = \sum_n a_n(t)\phi_n(\boldsymbol{r}) \tag{6}$$

where $\phi_n(\boldsymbol{r})$ represents the eigenfunction of the system of order *n*. For the sake of simplicity, assuming one group of delayed neutrons, a homogeneous reactor, and one-group diffusion theory, one could demonstrate that (the interested reader is referred to Lamarsh (2002) for the derivation of the following equations):

$$a_n(t) = A_n \exp(\omega_n t) \tag{7}$$

where A_n is a constant, and ω_n fulfils the following "in-hour" equation:

$$\rho_n = \frac{\omega t_n}{1+\omega t_n} + \frac{\omega}{1+\omega t_n}\cdot\frac{\beta}{\omega+\lambda} \tag{8}$$

with

$$t_n = \frac{1}{v(\Sigma_a + B_n^2 D)} \tag{9}$$

and B_n^2 is the geometrical buckling corresponding to the eigenmode *n*. One can easily show that

$$\omega_1 < \omega_0 \tag{10}$$

$$...\omega_2 < \omega_1 < 0 \tag{11}$$

and ω_0 is the only of the ω_n that can be positive.

For the global (in-phase) oscillation, the flux is oscillating over the whole core at a typical frequency of 0.5 Hz, and only the first neutronic mode (fundamental mode), i.e.

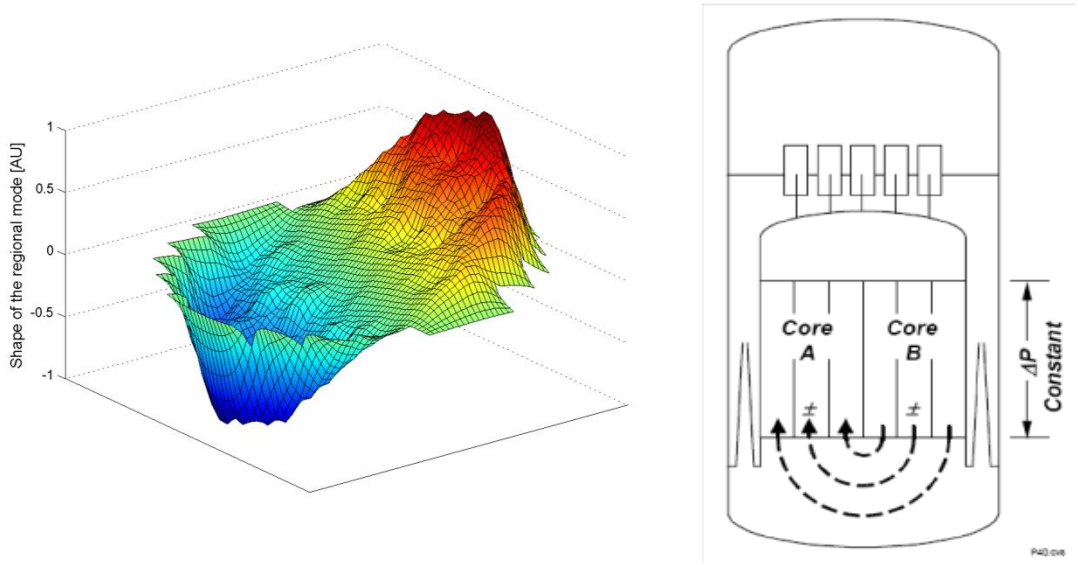

Fig. 5. Space dependence of the neutron noise induced by a regional oscillation as calculated by the neutron noise simulator (on the left hand-side) and conceptual illustration of the out-of-phase behavior of the flow and power oscillations (on the right hand-side) (from Siralkar, 2005)

$n = 0$, is excited. This is explained by the fact that the reactivity ρ_0 of the fundamental mode is the only one that can be larger than zero and correspondingly w_0 can be positive. The space-dependence of the flux is thus following the first neutronic mode. Due to the global character of the perturbation, the flow oscillations induced by the void/pressure oscillations are damped by the friction in the recirculation loop, and the recirculation loop dynamics has a stabilizing effect. The neutron noise induced by such an instability can be modelled by the neutron noise simulator, since the different eigenfunctions can be estimated by this tool. An example of the results of such a modelling is presented in Fig. 4.

For the out-of-phase (regional) oscillation, the second and third neutronic mode (first and second azimuthal modes), i.e. *n* = 1 and 2, are excited. Such modes are subcritical and should decay in time in an exponential manner. Nevertheless, the excitation of such modes leads to positive flow rate perturbations in one half of the core counterbalanced by negative flow rate perturbations in the other half of the core at any time in such a way that the boundary conditions imposed by the recirculation loop are always fulfilled. As a consequence, such oscillations are self-sustained by the thermal-hydraulics. The neutron noise induced by such an instability can also be modelled by the neutron noise simulator. An example of the results of such a modelling is presented in Fig. 5. One characteristics of the regional oscillation is that several higher modes can be excited, compared to only one for the in-phase oscillation. Typically, the second and third modes, i.e. first and second azimuthal modes respectively, are excited. Even if these modes are subcritical, the thermal-hydraulics might self-sustain the oscillations. The oscillation frequency of these two modes, although typically close to 0.5 Hz, might be slightly different from each other. Thus, the resulting oscillation, which is the sum of these two modes, might exhibit a rotating neutral line, with the neutral line being defined as the

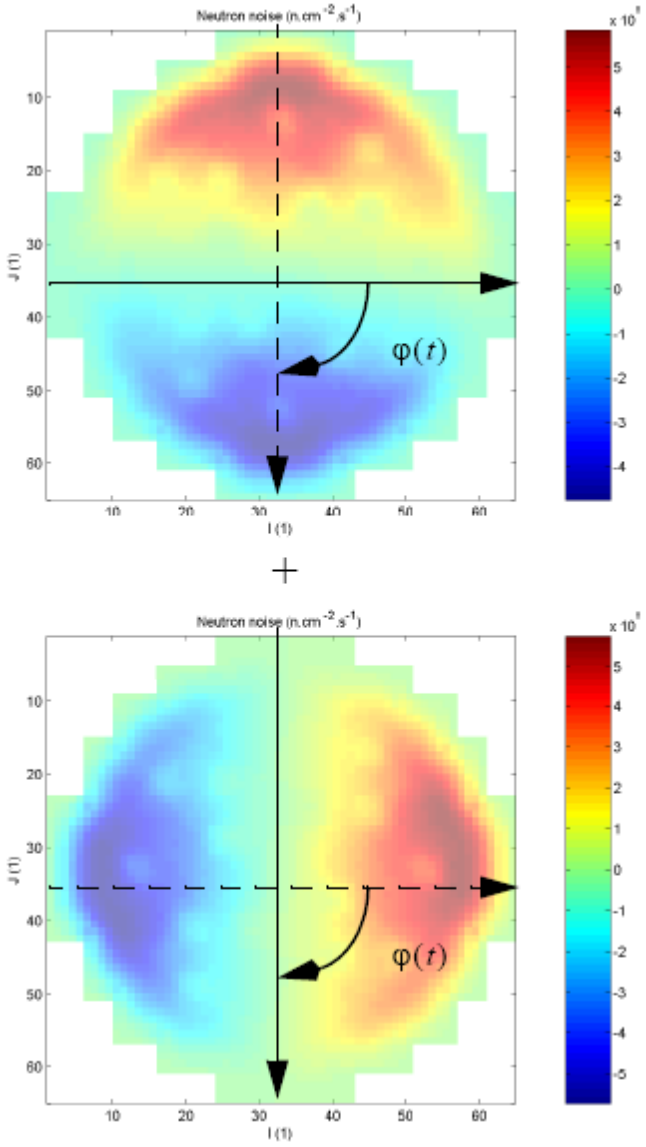

Fig. 6. Definition of the time-dependent phase shift between the first and second azimuthal modes

line separating the positive and the negative lobes of the oscillation. An equivalent formulation is to say that there exists a phase shift between the first and second azimuthal modes, and that this phase shift is time-dependent, as illustrated in Fig. 6. Very often, a fourth mode, i.e. the first axial mode, can also be excited. The regional or out-of-phase oscillation is thus a complicated oscillation due to its spatial intermittence, i.e. the neutral line might be stable or it might rotate.

1.6 Combined types of oscillations

When instability events occur at nuclear power plants, several types of oscillations are usually excited simultaneously, even if typically only one is predominant. This complicates significantly the estimation of the DR, since as explained earlier, the DR is

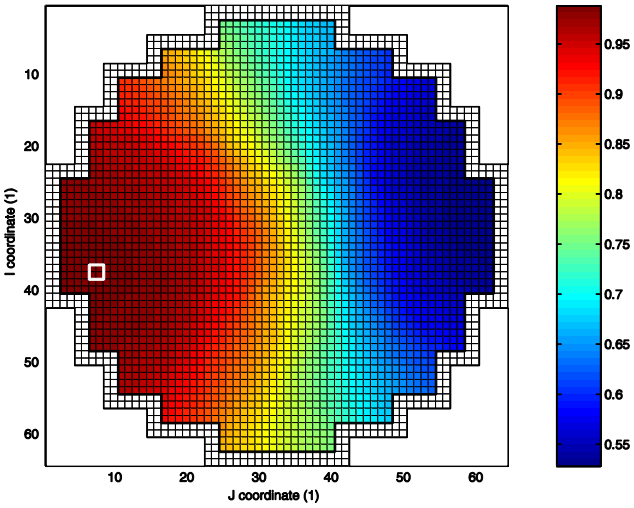

Fig. 7. Simulated radial space-dependence of the Decay Ratio in case of a local noise source and a global noise source (the white square represents the location of the local noise source)

based on the assumption that only one type of oscillation exists. Furthermore, it is customary to estimate the DR from the LPRMs, i.e. a value of the DR is estimated for each LPRM. One direct consequence of using local measurements for estimating a global parameter such as the DR is that the estimations might exhibit a space-dependence.

If only one type of oscillation is excited, then the DR is the same throughout the core. If several types are excited, the DR might become space-dependent. This can be demonstrated by assuming that the oscillations of the neutron flux can be written as a sum of the contributions of two oscillating modes, due to two different noise sources i $(i=1,2)$, each of them being factorized into a temporal part only and spatial part only $(\varphi_i(\boldsymbol{r}))$. In such a case, the DR, defined as the ratio of the first and the second maxima of the ACF, is given by (Pázsit, 1995):

$$DR(\boldsymbol{r}) = \sum_{i=1}^{2} c_i(\boldsymbol{r}) \cdot DR_i \tag{12}$$

with

$$c_i(\boldsymbol{r}) = \frac{1}{1 + C \cdot \dfrac{\varphi_j(\boldsymbol{r})}{\varphi_i(\boldsymbol{r})} \cdot \dfrac{\mathrm{In}(DR_i)}{\mathrm{In}(DR_j)}} \quad , \quad i \neq j \tag{13}$$

This expression was obtained assuming that each oscillation mode i has the same resonance frequency but different stability properties, i.e. DRs. Furthermore, it was supposed that the CPSD between the two noise sources is negligible, and that the DR of any of the two noise sources was larger than 0.4. $\varphi_i(\boldsymbol{r})$ represents the radial space-dependence of the neutron noise induced by the noise source *i*. This spatial dependence can be estimated by the neutron noise simulator for all types of BWR instabilities

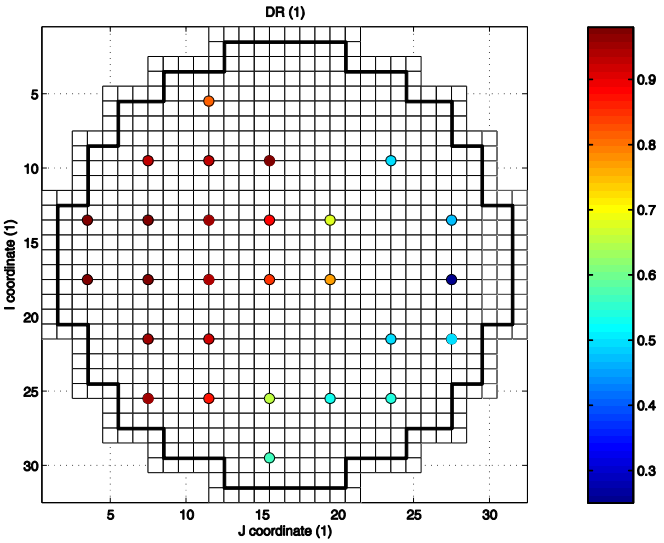

Fig. 8. Radial space-dependence of the DR determined at the Forsmark-1 BWR during the 1996/1997 channel instability (derived from Oguma, 1997)

(global, regional, or local oscillations). The coefficient C represents the ratio between the strength of the noise sources and is a normalization coefficient. The DR exhibits a strong radial space-dependence only when there are at least two types or sources of instabilities in the core with different stability properties, and at least one of those correspond to a local oscillation.

The case of a local oscillation coexisting with a global oscillation is shown in Fig. 7. The reason of the sharp boundary between the two stability regions when at least one local noise source exists is the fast spatial decay of the amplitude of the local oscillations. Such a pattern for the spatial dependence of the DR was actually noticed at the Forsmark-1 BWR, as can be seen in Fig. 8, during the channel instability event already mentioned in 2.5c(i) (the interested reader is referred to Oguma, 1997). Eqs (12) and (13) allow explaining the space-dependence of the DR in the Forsmark case, since a local oscillation could be triggered by an unseated fuel assembly.

In order to correctly estimate the stability properties of a BWR, it is thus essential to separate the different types of oscillations from each other. Thereafter, the stability of each mode can be characterized by a DR per oscillation mode. Different techniques have been elaborated for monitoring the stability of BWRs and for separating the different modes of oscillations.

Whereas the global oscillations can be properly detected by the Average-Power Range Monitors (APRMs), the LPRMs are necessary to characterize the regional oscillations. The monitoring techniques that are capable of detecting different types of oscillations can basically be classified into three categories, which are briefly explained in the following in increasing order of sophistication.

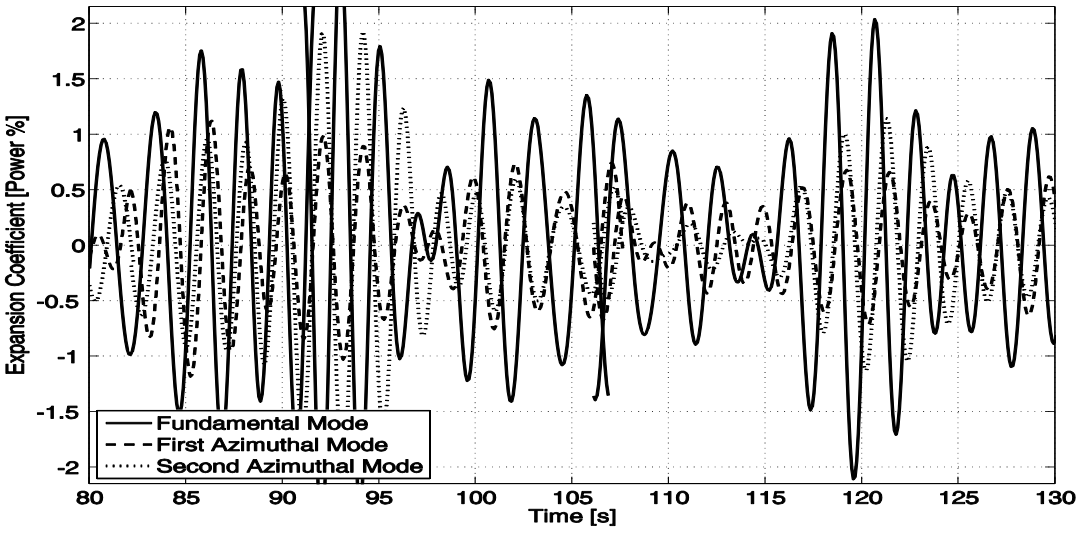

Fig. 9. Time-dependence of the expansion coefficients for the three first modes applied to the LPRM signals during a stability test at the Ringhals-1 BWR

The first class of techniques aims at monitoring the phase difference between pairs of symmetrically-located LPRM detectors. A phase shift approaching 180 deg indicates out-of-phase oscillations, whereas a negligible phase shift indicates in-phase oscillations. The drawback of these techniques is the difficulty in monitoring combined modes of oscillations.

The second category of techniques is based on the determination of the part of the LPRM signals related to the in-phase oscillations, using for instance the property of orthogonality between the fluctuations of the shape function of the neutron noise and the static flux. This leads to

$$\frac{\delta P(t)}{P_0} = \frac{\delta \phi^{pk}(\boldsymbol{r},t)}{\phi_0(\boldsymbol{r})} = \frac{\int \delta\phi(\boldsymbol{r},t)\phi_0(\boldsymbol{r})d\boldsymbol{r}}{\int \phi_0^2(\boldsymbol{r})d\boldsymbol{r}} \tag{14}$$

Subtracting this in-phase component to each of the LPRM signals also allows detecting possible out-of-phase oscillations.

The last class of techniques is based on modal decomposition of the neutron noise. In this procedure, the neutron flux is expanded in the eigenfunctions of the system as:

$$\bar{\phi}(t) = \sum_n a_n(t)\bar{\phi}_n \tag{15}$$

with

$$a_n(t) = \frac{\left\langle \bar{\phi}_n^{\dagger}, \bar{\bar{F}} \times \bar{\phi}(t) \right\rangle}{\left\langle \bar{\phi}_n^{\dagger}, \bar{\bar{F}} \times \bar{\phi}_n \right\rangle} \tag{16}$$

In these equations, the vector $\bar{\phi}(t)$ represents the space- and time-dependent neutron flux (where each element of the vector represents the value of the time-dependent flux at a spatial point in the system), $\bar{\phi}_n$ represents the space-dependent eigenfunction of mode *n*, $\bar{\phi}_n^{\dagger}$ is its adjoint, and $\bar{\bar{F}}$ is the fission operator. This decomposition can be performed either with the prior determination of the different modes of the static neutron flux or without it. An example of such a modal decomposition applied to a stability test performed at the Swedish Ringhals-1 BWR is represented in Fig. 9. As can be seen in this figure, both the global and the regional oscillation patterns are excited in the analysed stability test. It is interesting to notice that both the global and regional oscillations are clearly intermittent, and that they sometimes exhibit growing amplitudes over a couple of periods. Furthermore, it can also be seen that the phase shift between the first and second azimuthal modes is varying with time. As a consequence, the regional oscillation, which is a combination of these two azimuthal modes, will be characterized by a rotating neutral (nodal) line.

2 An investigation of the significance of the properties of the noise source for BWR instability

2.1 Introduction

In conceptual interpretation of the stability properties of boiling water reactors often a simplified model is used which assumes that the power or flux oscillations in the core can be described as the response of a damped linear oscillator, driven by a white noise driving force. It is obvious that such a model describes the behaviour of the system only in the linear regime, whereas fully developed instabilities are non-linear in character. However, such a model still proves useful in understanding the path to instability, especially the interplay of several different oscillation modes (global, regional, local) (Pázsit, 1995; Demazière and Pázsit, 2005). In such models of the BWR dynamics, it is always assumed that the driving force has a white noise spectrum, i.e. it is constant in frequency. However, the situation becomes different if the APSD of the driving force has a frequency dependence (``coloured noise''). In principle there are two situations when estimating system properties with the assumption of white driving source can lead to erroneous estimation of the decay ratio. One is if the driving force has resonances of its own, which can be interpreted as system resonances. Such resonances are known to occur in form of standing waves in the primary circuit of PWRs, and their presence can complicate the understanding of the properties of the flow induced vibrations of PWR internal structures. A slight resonance of the driving force close to the oscillation frequency of the system resonance can shift into the system frequency due to change in the parameters determining the force properties. This would then occur as a change in the system properties (stability). Another possibility is if the driving force has a sink (dip) at the system resonance that leads to a resulting system response which, when interpreted as only due to system properties as induced with a white driving force, would indicate a stable system. This should be a potentially dangerous situation, since the presence of an instability would not be observed until there is a shift in the sink frequency of the driving force, leading then to a much more unstable system behaviour.

The driving force in our model is represented by the reactivity perturbation, which are generated by the propagating density fluctuations of the two-phase flow. The thought on the possible role of the changed properties of a none-white driving force is supported by the fact that the instability occurs at a certain point of flow and power values on the power-flow map, and disappears when the operational point is moved on the map. This may be primarily due to the dependence of the system properties on the flow conditions. However, according to the above reasoning, the properties, and in particular the sink structure of the driving force, are also changing with the changes in flow velocity. Then, the change in the stability properties of the system response may be influenced also by the properties of the driving force.

Assuming that the driving force has a frequency spectrum equal to that of the reactivity effect of propagating two-phase flow the system response to such a perturbation, and in particular the ACF (auto-correlation function) of the response can be calculated analytically. This will be described in the following sections. The response is then compared to that obtained from the same system with a white driving force, and the

possible error in the estimation of the system response by assuming a white driving force is calculated.

2.2 Calculations for a white noise driving force

The solution of this classic case has known been long, and one re-derivation is found e.g. in (Pázsit I. (1995)). Since a similar methodology will be used for the case of a coloured noise driving force, we briefly repeat here the main steps of the calculation. The damped oscillator is described by the second order equation:

$$\delta\ddot{\phi}(t) + 2\xi\omega_0\delta\dot{\phi}(t) + \omega_0^2\phi(t) = f(t). \tag{17}$$

where $f(t)$ stands for the driving force. With a temporal Fourier transform of (17) and using the Wiener-Khinchin theorem, one obtains APSD of $\delta\phi(\mathbf{r},t)$ as:

$$APSD_{\delta\phi}(\omega) = APSD_f \mid H(\omega) \mid^2 = \frac{C}{(\omega_0^2 - \omega^2)^2 + 4\xi^2\omega^2\omega_0^2}, \tag{18}$$

where C stands for the constant APSD of the driving force and $H(\omega)$ is the system transfer function. The autocorrelation function is obtained by an inverse Fourier transform of $APSD_{\delta\phi}(\omega)$, for which the poles of $|H(\omega)|^2$ need to be determined. If one only considers cases when the decay ratio $\beta = e^{-\xi 2\pi} \geq 0.5$, then neglecting terms of $O(\xi^2)$ besides unity, the APSD poles can be presented as:

$$\omega_{1,2,3,4} = \pm\omega_0(1 \pm i\xi).$$

The ACF can now easily be calculated by the theorem of residues. The details are not given here since the calculation is straightforward. For the numerical values of ξ that are usually encountered, the result is given as

$$ACF(\tau) = \frac{C\, e^{-\xi|\tau|\omega_0}}{4\xi\omega_0^3}\cos(\tau\omega_0). \tag{19}$$

The form Eq.(19) will be used to determine the decay ratio and resonance frequency from the noise induced by a coloured driving force in the forthcoming analysis.

2.3 The reactivity effect of propagating perturbations: a non-white driving force.

Now we consider the case of a driving force with non-constant spectral content. The spectral form of the driving force will be taken as the reactivity effect induced by a propagating perturbation with a white noise at the inlet. This type of driving force was studied extensively in the early 70'es as a model for the reactivity perturbations induced by the inlet temperature fluctuations of the coolant in a PWR (Kosály. and Williams, 1971; Kosály and Meskó, 1972; Pázsit, 2002). The model used in the above publications assumes that the perturbations entering the inlet propagate axially along the whole height of the core unchanged which is not really valid for two-phase flow. However, some basic features of the perturbation, such as the presence of peaks and sinks (will be seen below), are expected also from the boiling noise. At any rate, this appears to be a suitable model for a non-white driving force with some relevance to realistic cases.

As is described in the above publications, the propagating perturbation is defined by the relationship:

$$\delta\Sigma_a(z,t) = \delta\Sigma_a\left(0, t - \frac{z}{v}\right). \tag{20}$$

From here it follows that the frequency dependence of $\delta\Sigma_a(z,t)$ is given as:

$$\delta\Sigma_a(z,\omega) = \delta\Sigma_a(0,\omega)e^{-\frac{i\omega}{v}z}. \tag{21}$$

Then, the reactivity in first order perturbation theory is defined as:

$$\rho(t) = -\frac{1}{v\Sigma_f}\int_0^H \phi^2(z)\delta\Sigma_a(z,t)dz, \tag{22}$$

which in the frequency domain becomes:

$$\rho(\omega) = -\frac{\delta\Sigma_a(0,\omega)}{v\Sigma_f}\int_0^H \phi^2(z)e^{-\frac{i\omega}{v}z}dz. \tag{23}$$

From here, with an application of the Wiener-Khinchin theorem and using the normalized flux $\phi(z) = \sqrt{\frac{2}{H}}\sin\frac{\pi}{H}z$, , one obtains the following expression for reactivity APSD:

$$APSD_\rho(\omega) = \frac{32k^2\pi^4v^6(1-\cos\omega T)}{(v\Sigma_f)^2H^4\omega^2\ \left(\omega^2-\omega_T^2\right)^2}. \tag{24}$$

where $T = H/v$ and $\omega_T = 2\pi/T = 2\pi v/H$. Here T stands for the transit time of the perturbation in the core and ω_T is the corresponding angular frequency. As is easy to show, the function above has no poles at $\omega = 0$ and $\omega = \omega_T$. On the other hand, $APSD_\rho(\omega)$ has a sink structure, i.e. has zeros at:

$$\omega_n = n\omega_T; \qquad n = 2,3,\ldots \tag{25}$$

An illustration of this APSD is shown in Fig. 10 as a function of the frequency.

The transit time was selected as $T = 2$ sec, which is a typical value of the coolant in BWRs, leading to the characteristic frequency $f_T = \frac{\omega_T}{2\pi} = 0.5$ Hz. Hence the sink frequencies f_n are equal to $f_n = n\,f_T$, $n = 2,3\ldots$. According to experience, the core resonance frequency f_0 is also equal to the inverse of the transit time of the coolant in the core, so that $f_T = f_0$, or $\omega_T = \omega_0$. However, in the investigation of the properties of the induced noise, we will decouple these two variables and investigate cases when they are not equal to each other.

Interestingly, the autocorrelation function of this reactivity APSD of the propagating perturbations was never written down. One way to do that is the Fourier-inversion of (24) which is not trivial, and will be implemented in the next Section. Alternative way is based on the observation that the white noise character of $\delta\Sigma_a(0,t)$ can be expressed by:

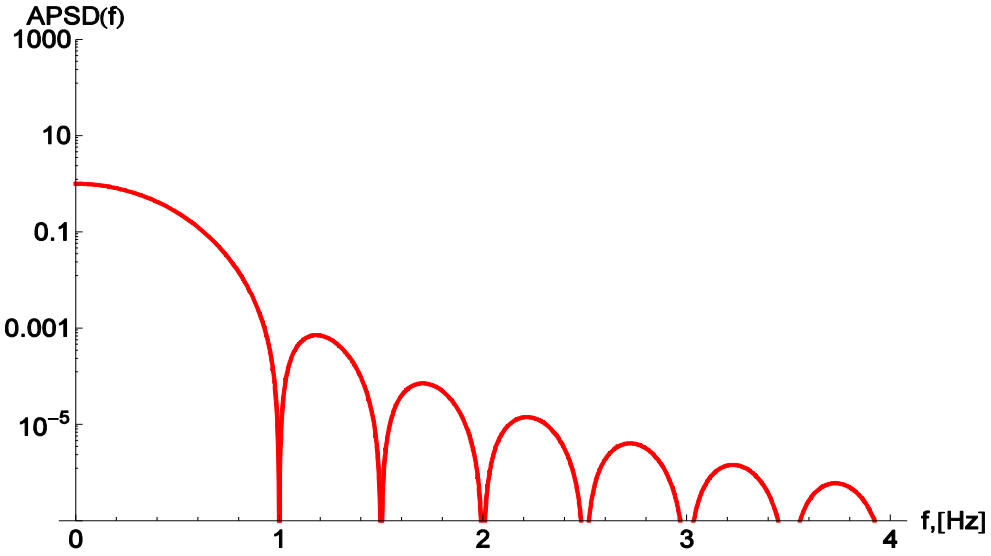

Fig. 10. APSD of the reactivity fluctuations due to propagating perturbations $\mathrm{T} = 2\,s$, $f_T = 0.5\ Hz$.

$$< \delta\Sigma_a(0,t)\delta\Sigma_a(0,t') >= k^2\delta(t-t'). \qquad \textbf{(26)}$$

Then, writing $t' = t + \tau$ and utilizing the traditional definition of ACF as a time convolution, one has:

$$ACF_\rho(\tau) = \begin{cases} \dfrac{\nu k^2}{(\nu\Sigma_f)^2}\displaystyle\int_0^H dz\phi^2(z)\phi^2(z+|\tau|\nu) & \text{if} \quad |\tau| < T. \\ 0 & \text{if} \quad |\tau| \geq T \end{cases} \qquad (27)$$

Physically, this means that since the perturbation enters at the inlet with a zero correlation time (white noise), spatial correlations of the noise can only be found between points that belong to the same entry, and such can only be found for time differences less or equal to the time *T* of the perturbation passing the core, which is therefore the maximum correlation time of the driving force.
Performing the integral leads to the final result:

$$ACF_\rho(\tau) = \frac{\nu k^2}{2(\nu\Sigma_f)^2 H^2}\left\{(H-|\tau|\nu)(2+\cos\omega_T\tau) + \frac{3H}{2\pi}\sin\omega_T|\tau|\right\}\theta(T-|\tau|). \qquad (28)$$

Some examples of this autocorrelation function are shown in Fig. 11.

2.4 Calculations for the non-white driving force.

We will now assume that the APSD of the driving force $f(t)$ of Eq. (17) has the same functional form, i.e. the same frequency dependence as that of the reactivity

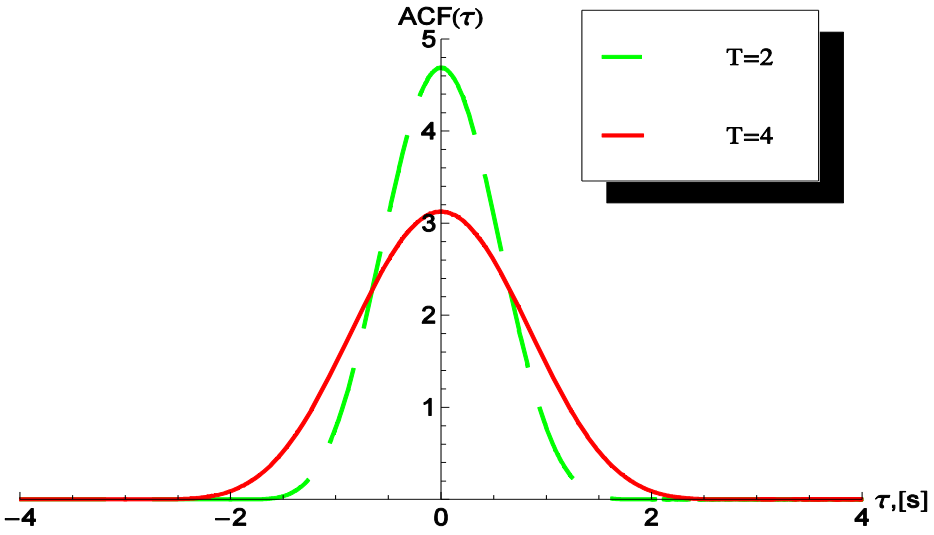

Fig. 11. The ACF of the reactivity effect of propagating perturbations for two different transit times.

perturbations, but we omit the constant factors such that the notations become simpler. Then one has:

$$APSD_f(\omega) = \frac{1-\cos\omega T}{\omega^2(\omega^2-\omega_T^2)^2}. \qquad (29)$$

With this APSD of the driving force one obtains for $APSD_{\delta\phi}$ the expression:

$$APSD_{\delta\phi}(\omega) = APSD_f(\omega)\,|H(\omega)|^2 = \frac{(1-\cos(\omega T))}{\left[(\omega_0^2-\omega^2)^2+4\xi^2\omega^2\omega_0^2\right]\omega^2(\omega^2-\omega_T^2)^2}, \qquad (30)$$

where $APSD_f$ is given by (29), and the transfer function $H(\omega)|$ is the same as given before.

Determination of the ACF from (30) with inverse Fourier transform goes along the same lines as before. One needs to determine the poles of $APSD_{\delta\phi}$. These come partly from the poles of $|H(\omega)|^2$ which are the same as before and partly from $APSD_f$, which are quite specific and create some peculiarities in ACF function.

Namely, it can be shown that for the asymptotic part of the ACF, defined as the part of the curve for $\tau > T$, the ACF will show exactly the same decaying oscillation character, and hence also lead to the same decay ratio, as with a white noise driving force. Consequently, it will also show the true decay ratio. That happens since $APSD_f$ doesn't give any contributions into poles for $\tau > T$ but does for $\tau < T$. In a general setting this result means that the ACF of the noise oscillations induced by a coloured driving force will deviate from those induced by a white driving force over the correlation time of the driving force. We will call this the transient part of the ACF. If this correlation time is finite, as in the present case, then the transient part will be finite, followed by an asymptotic part of the ACF of the induced neutron noise which will not differ from that induced by a white noise driving force.

The calculations needed for the Fourier inversion of (30) were performed by using Mathematica. After extensive algebra, for the case of small ξ as in the case of the white driving force, one obtains:

$$\begin{aligned} ACF(\tau) &= e^{-\xi\omega_0|\tau|}A\cos\ \omega_0|\tau|-\alpha\ \Theta[|\tau|] \\ &-0.5e^{-\xi\omega_0|T-\tau|}A\cos\ \omega_0|T-\tau|-\alpha\ \Theta[|\tau-T|] \\ &-0.5e^{-\xi\omega_0|T+\tau|}A\cos\ \omega_0|T+\tau|-\alpha\ \Theta[|\tau+T|] \\ &+\frac{T^4}{128\pi^5}\left((T-|\tau|)(\frac{4\pi}{\omega_0^4}+F\cos\ \omega_T\tau\ )+Y\sin\ \omega_T|\tau|\ \right)\Theta[T-|\tau|], \end{aligned} \tag{31}$$

Where A_1, B_1, F, Y are complicated functions of system parameters ξ, ω_0, T.
The correctness of the above solution was checked both by Fourier-transforming it back to the frequency domain by Mathematica, and by calculating the inverse Fourier transform of (30) with a numerical FFT routine and comparing it with (31).

2.5 Analysis of the results

We shall now analyse the results both qualitatively and quantitatively for case when $f_0 = f_T = 0.5$ Hz, corresponding to a transit time of $T = 2$ sec. The corresponding APSD of the driving force was shown in Fig. 10. From the stability point of view this frequency spectra can demonstrate two interesting cases: one when we have a strongly damped system (fast decaying ACF, low decay ratio) corresponds to a wide peak in the system transfer APSD, and an unstable system (slowly decaying ACF) corresponds to a narrow resonance. At the same time, the corresponding "measured" ACF will be different from that of the transfer function alone. We shall call this the virtual APSD or ACF, as opposed to the ``true" one which belongs to the transfer function. Namely, if the driving force has a narrow resonance around the peak frequency of the system resonance, then the "virtual" APSD will be narrower (higher decay ratio), than that of the true system, meaning better system stability than the one deduced from the measurements. From the operating point of view, on the other hand, this situation is disadvantageous, since the load on the system due to the large amplitude power oscillations is just as large as in the case of high true DR.

The other possibility of a significant difference between the virtual and the true stability is when the APSD of the driving force has a deep local minimum at the peak frequency of the system resonance. In that case the peak of the induced noise APSD will be broader than that of the system resonance, hence the stability deduced from the measurements is larger than the true one (the virtual DR is smaller than the true one). This means that the driving force in this case suppresses the power oscillations, which is advantageous for the operation. The potential danger of the situation is that a possibly highly unstable state of the system goes unnoticed. However, none of the above cases occurs in our model ($\omega_0 = \omega_T$, $f_0 = f_T$) which can be seen in Fig. 12 with a true DR of the system being equal to 0.8. As seen from the Figure, since the driving force has the first sink at $2f_T$, the frequency dependence of the driving force is smooth over the resonance frequency f_0, without any peaks. Consequently, the width of the resonance of the measured signal (the ``virtual" resonance) is very similar to that of the system

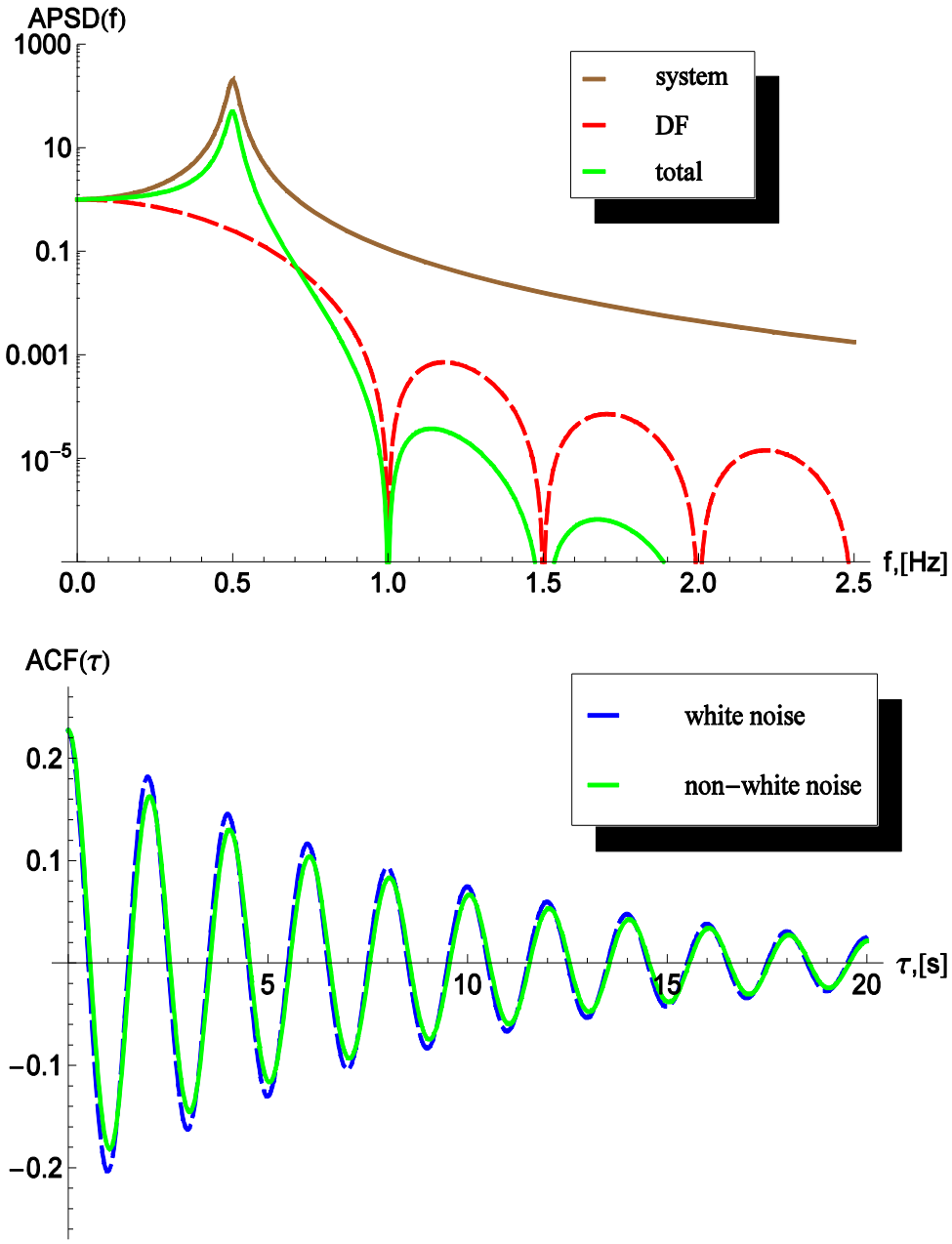

Fig. 12. APSD and ACF of the system transfer and the total resulting noise for $f_T = f_0 = 0.5$ *Hz for the case of* $DR = 0.8$.

resonance. In that case, having DR=0.8, the resonances for both the system and the arising noise are relatively narrow.

One can study various further cases by keeping f_0 constant and changing f_T .Increasing f_T will not yield any qualitatively new result simply giving smoother behaviour of the noise source APSD over the system resonance at f_0. A more interesting case is when f_T is decreased, such that the first sink of the driving force starts to approach the resonance of the transfer function. At $f_T = f_0 / 2$ the first sink of the APSD of the driving force

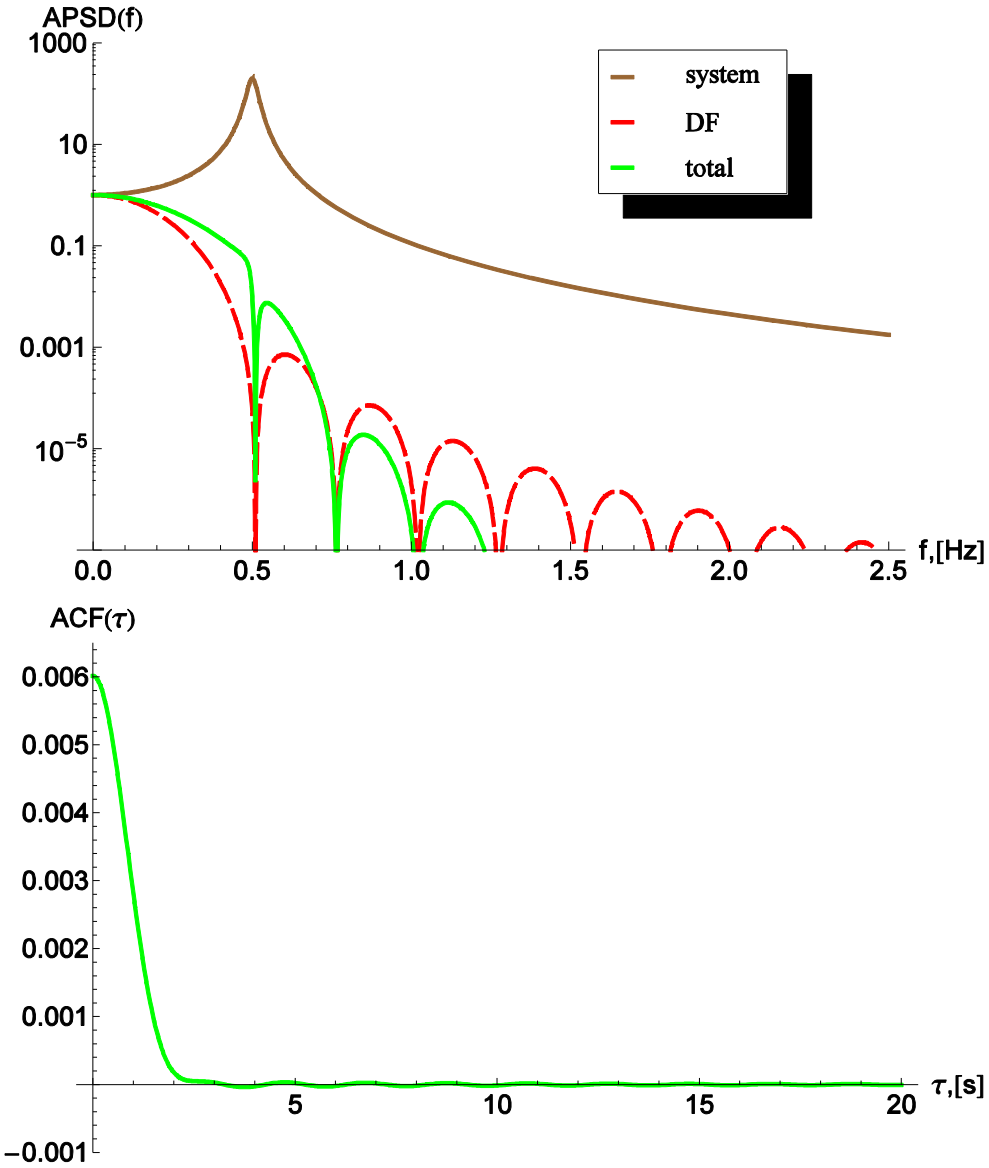

Fig. 13. APSD and ACF of the system transfer and the total resulting noise for $f_T = 0.51 f_0$ *for the case of* $DR = 0.8$.

coincides with the resonance of the system transfer function. In that case the resulting noise will actually have a dip instead of a maximum (Fig. 13, upper figure). In these cases, on the face of it, the ACF indicates a high stability in that the ACF actually does not even show oscillations (Fig. 13). (Due to the large difference between the ``true'' and the ``virtual'' ACFs, only the latter is shown in this case). Such curves are actually observed in some measurements. According to the model cases studied here, this can happen with a coloured driving force even in cases when the system DR is relatively high.

In practice such a situation might cause a problem. Although, as it was mentioned earlier, the asymptotic decay ratio even for this case is equal to the true one, in a realistic case of using measured data, the oscillations of the asymptotic part of the ACF would be completely masked with measurement scatter and background noise. This

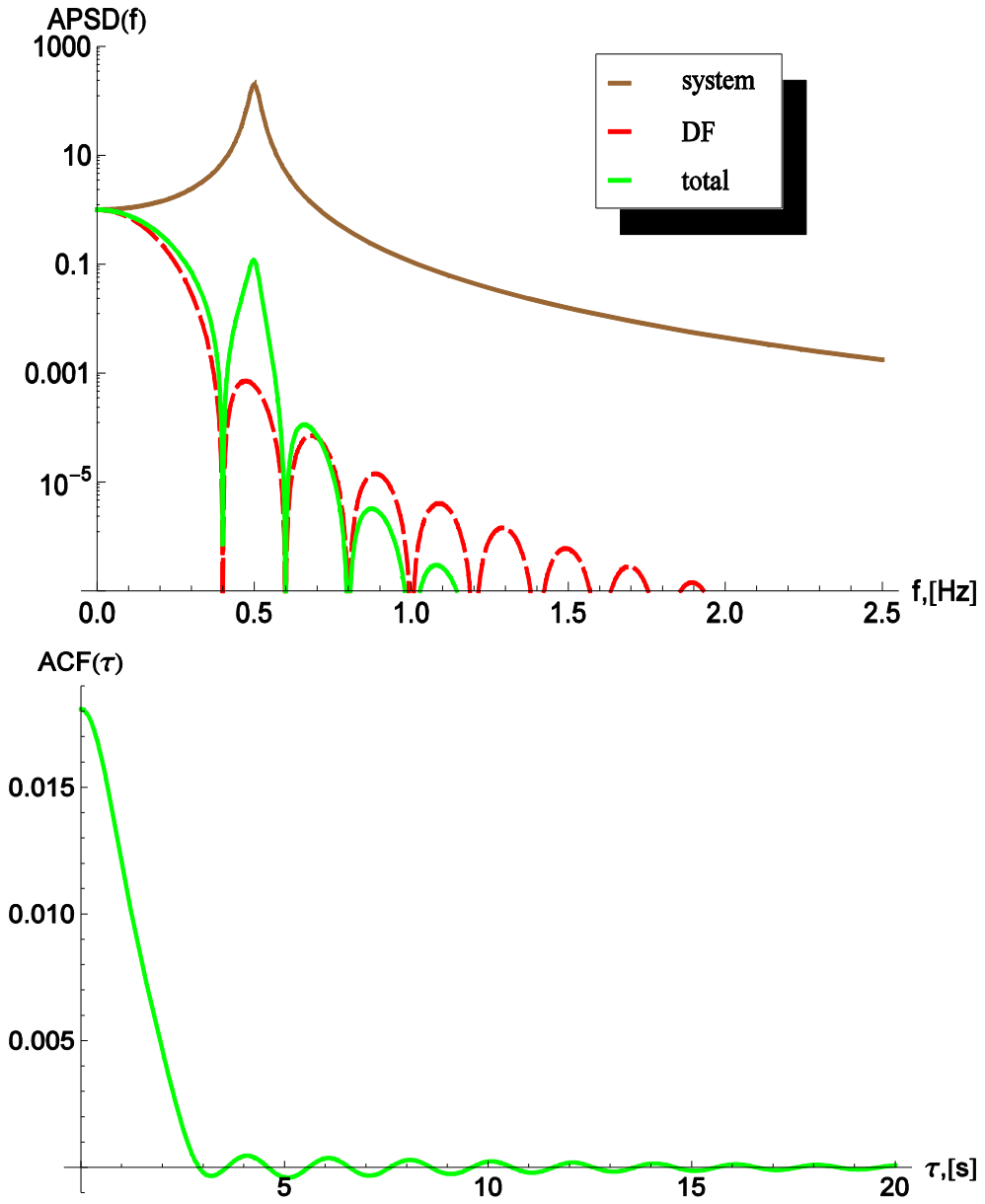

Fig. 14. APSD and ACF of the system transfer and the total resulting noise for $f_T = f_0 / 2.5$ *for the case of* $DR = 0.8$.

means that the asymptotic decay ratio cannot be determined, only the virtual one based on the first part of the ACF, making the presence of an unstable system dynamics impossible to discover. The problem with such a situation is that a change in the thermal hydraulic parameters such that f_T moves away from its value will result in the fact that the possible unstable state of the system is uncovered. This could appear as one possible explanation of a decay ratio strongly dependent on the coolant velocity in certain cases.

Finally we show the case of $f_T = 2.5 f_0$ (Fig. 14), in which case the first local maximum of the driving force APSD coincides with a system resonance. Due to the relatively large value of T as compared to T_0, several oscillations of the ACF of the system transfer function are now covered by the transient part of the curve.

As mentioned earlier, although the asymptotic decay ratio DR_{asy}, defined as the decay ratio determined from the asymptotic part of the ACF, i.e. for $\tau > T$, would yield a correct result, in practice there are several circumstances that might make the determination of this parameter complicated. One is the fact that in a measurement it is not known in advance how large the transient region of the ACF is. The second is that the asymptotic part can have a small amplitude and the only way of determining the decay ratio is to use the whole ACF. For this reason it might be interesting to investigate the magnitude of the error of determining the decay ratio from the measured ACF in case of a coloured driving force. Thus a series of calculations were made for various values of the true DR and various values of T (and hence f_T) of the model of the driving force. The decay ratio was determined from the ACF of the induced noise by curve fitting in two ways: partly for the whole curve, including the transient part (denoted as DR_{tr}), and partly from the asymptotic part of the ACF only, denoted as DR_{asy}.

The results for the various cases are summarized in Table 1. As can be expected, in the idealised case of having access to the whole ACF without measurement uncertainties, interfering processes etc., the asymptotic decay ratio always coincides with the true one. The fitting to the whole curve, on the other hand, can lead to large deviations from the true DR, significantly underestimating it. Hence the presence of the coloured driving force has a tendency of inducing a non-conservative error in the estimate. The fitting also serves the resonance frequency, kept constant at 0.5 Hz in these calculations, which is always correctly obtained by both curve fitting procedures.

2.6 Conclusions

Through a simplified model of the non-white character of the driving force for global BWR oscillations, i.e. the reactivity noise of propagating perturbations, the deviation of the system response from that induced by a white noise driving force, resulting in a response identical with the system transfer function, was quantified. It was found that for the cases observed in practice so far, where the system resonance frequency is equal to the inverse of the transit time of coolant through the core, the non-white character of the driving force induces negligible changes in the induced neutron flux oscillations as compared to those induced by a white noise driving force. However, it was shown that in the somewhat pathological case when a dip of the driving force coincides with the system resonance, the induced noise indicates a completely stable system even in case of an unstable one.

One conclusion is that at least with the model of the driving force chosen, in practical cases the deviation from the noise induced by a white noise driving force is negligible. However, other types of non-white driving force cannot be excluded, hence the investigations in this work might give some hint of the effects that can be expected. It is also interesting to note that in reality the measured ACFs often deviate from the ideal second order system, and the ACFs calculated here with the non-white driving force managed to reproduce such features.

Table 1. Results of curve fitting with the ACF of white driving force, Eq. (19), to the ACFs with non-white driving force spectra.

	Decay ratio			Frequency, Hz		
	DR	DR_{tr}	DR_{asy}	f_0	f_T	f_p
Case1. $DR = 0.6$						
$f_T = f_0 = 0.5$ Hz	0.6	0.57	0.6	0.5	0.5	0.5
$f_T = \frac{2}{3} f_0 = 0.33$ Hz	0.6	0.38	0.6	0.5	0.49	0.5
$f_T = 0.55 f_0 = 0.29$ Hz	0.6	0.11	0.6	0.5	0.5	0.5
$f_T = 0.51 f_0 = 0.26$ Hz	0.6	0.085	0.6	0.5	0.49	0.5
$f_T = 0.5 f_0 = 0.25$ Hz	0.6	0.059	0.6	0.5	0.5	0.5
$f_T = 2.5 f_0 = 0.2$ Hz	0.6	0.15	0.6	0.5	0.49	0.5
Case2. $DR = 0.8$						
$f_T = f_0 = 0.5$ Hz	0.8	0.8	0.8	0.5	0.5	0.5
$f_T = \frac{2}{3} f_0 = 0.33$ Hz	0.8	0.65	0.8	0.5	0.51	0.5
$f_T = 0.55 f_0 = 0.29$ Hz	0.8	0.21	0.8	0.5	0.5	0.5
$f_T = 0.51 f_0 = 0.26$ Hz	0.8	0.14	0.8	0.5	0.5	0.5
$f_T = 0.5 f_0 = 0.25$ Hz	0.8	0.1	0.8	0.5	0.5	0.5
$f_T = 2.5 f_0 = 0.2$ Hz	0.8	0.31	0.8	0.5	0.5	0.5
Case3. $DR = 0.98$						
$f_T = f_0 = 0.5$ Hz	0.98	0.98	0.98	0.5	0.5	0.5
$f_T = \frac{2}{3} f_0 = 0.33$ Hz	0.98	0.97	0.98	0.5	0.5	0.5
$f_T = 0.55 f_0 = 0.29$ Hz	0.98	0.53	0.98	0.5	0.5	0.5
$f_T = 0.51 f_0 = 0.26$ Hz	0.98	0.23	0.98	0.5	0.52	0.5
$f_T = 0.5 f_0 = 0.25$ Hz	0.98	0.11	0.98	0.5	0.5	0.5
$f_T = 2.5 f_0 = 0.2$ Hz	0.98	0.61	0.98	0.5	0.51	0.5

3 Study of the dynamics of molten salt systems: construction of the adjoint and calculating the space dependent noise induced by propagating perturbations in the fuel

3.1 Introduction

In a previous report, Stage 13, a simple one-dimensional model with propagating fuel properties was set up and studied as a model of a molten salt reactor. The solution of the static eigenvalue equation was given first by expansions into eigenfunctions of a corresponding traditional reactor, i.e. an MSR with fuel velocity $u = 0$. Then the neutron noise generated by propagating perturbations was calculated in the point kinetic approximation. For this calculation, a simplified empirical model of the zero reactor transfer function $G_0(\omega)$, suggested by MacPhee (1958) and used by Dulla (2005), was investigated. The noise in the point kinetic approximation was studied in systems with propagating perturbations in the past, and it is known that this approximation predicts a periodic sequence of peaks and sinks in the frequency domain, arising from the properties of the perturbation.

The goal in Stage 14 was therefore to perform a quantitative analysis of the noise in the point kinetic approximation, with an extension to the case when there are several channels with different velocities, to see how the co-existence of several velocities distorts the known sink structure. At the same time we noted that the empirical model of the $G_0(\omega)$ for MSR contains some ripples which were not noted in the previous Stage. These are related to the recirculation time of the fuel, and to the transit time of the fuel in the core. The work in Stage 14 consists of both a quantitative analysis of the fine structure of the zero power reactor transfer function for MSR, and the frequency dependence of the noise induced by propagating perturbations in the point kinetic approximation. Several cases with different radial velocity distributions were investigated quantitatively.

In Stage 15 we turned to the solution of the space-dependent equations. A first idea was a rigorous derivation of the point kinetic approximation with the Henry factorisation procedure, but this was postponed because it requires the knowledge of the adjoint function. It turns out that the one-group diffusion equations for an MSR are not self-adjoint, due to the directed flow of the fuel. Hence for the MSR a method has to be found to define the adjoint, and this was postponed to the next Stage. The space-dependent equations were then solved for the Green's function of the system by the same eigenfunction expansion technique as in the static case. It turned out, however, that due to the discontinuity of the Green's function at the point of the perturbation, the solution for the noise equations with this method is much more complicated than in the static case. The quantitative results showed that the space dependence of the induced noise was not reliably reconstructed by the method, because of the need of very many terms to satisfy the discontinuity. The frequency dependence, on the other hand, was reliably reconstructed.

In Stage 15 therefore two paths were followed. Partly, the frequency dependence of the space-dependent Green's function was investigated in a few spatial points. A comparison with the empirical suggestion for the $G_0(\omega)$ showed that for cases where the space-dependent solution is expected to behave in a point kinetic way, i.e. for small reactors at low frequencies, the two solutions still differ significantly. This indicates the insufficiency of the empirical model.

The other path was to calculate the Green's function for infinite fuel velocity. For such a case, a compact analytical solution can be found with a method which is similar to the elimination of the uncollided flux in transport problems. The significance and use of such a solution arises from the fact that the case of infinite velocity can be considered as the maximum deviation from the traditional reactors in some sense, thinking of the fact that the k_{eff} of an MSR with all material and geometrical parameters constant behaves monotonically as a function of the fuel velocity. Hence the behaviour of the system as a function of system size and perturbation frequency can be studied and compared with traditional systems. The comparison showed that an MSR behaves point kinetically for higher frequencies or system sizes than a traditional reactor of equivalent parameters.

In Stage 16 first first the adjoint equations of the one-group diffusion theory are derived for reactors with moving fuel. The adjoint property of the suggested form is proven both for the differential form of the coupled neutron-precursor equations, and for the integro-differential form, obtained after eliminating the delayed neutron precursors. Then the Green's function of the reactor is calculated for finite fuel velocities, with the employment of a method, suggested in the previous Stage for the solution for infinite fuel velocities. The space and frequency dependence of the Green's function is investigated. Finally, the space-dependent noise, induced by propagating perturbations, are calculated and discussed. It is shown that with increasing fuel velocity, the behaviour of a given system at a given frequency tends to be more and more point kinetic, in accordance with the results for infinite fuel velocity, found in the previous Stage.

3.2 The adjoint function

The fact that the equations are not self-adjoint can be easily seen by writing the equations in matrix form:

$$\mathbb{M}\vec{\phi}_0(z) = \begin{pmatrix} D\nabla^2 + \nu\Sigma_f(1-\beta) - \Sigma_a & \lambda \\ -\nu\Sigma_f\beta & u\dfrac{\partial}{\partial z} + \lambda \end{pmatrix} \begin{bmatrix} \phi_0(z) \\ C_0(z) \end{bmatrix} = 0 \tag{32}$$

Then, it is easy to see that

$$\left\langle \vec{\Psi}_0(z)\mathbb{M}\vec{\phi}_0(z) \right\rangle \neq \left\langle \vec{\phi}_0(z)\mathbb{M}\vec{\Psi}_0(z) \right\rangle \tag{33}$$

where the brackets indicate integration over the core, i.e.

$$\left\langle \phi_0(z)\Psi_0(z) \right\rangle = \int_0^H \phi_0(z)\Psi_0(z)dz \tag{34}$$

The problem here is with the convection term for the precursors; all other terms

give equal contributions. Similarly to the case of the transport equation, in order to construct the adjoint equation and the adjoint flux, it is not sufficient to construct an adjoint operator; one also needs to specify boundary conditions for the adjoint flux (in the present case for the precursor densities).

Hence we seek a matrix $\mathbb{M}^{\dagger}$ such that

$$\left\langle \vec{\phi}_0(z)\mathbb{M}^{\dagger}\vec{\phi}_0^{\dagger}(z)\right\rangle = \left\langle \vec{\phi}_0^{\dagger}(z)\mathbb{M}\vec{\phi}_0(z)\right\rangle \tag{35}$$

From considering that the adjoint equation is related to time-reversal, the adjoint operator can be written as

$$\mathbb{M}^{\dagger} = \begin{pmatrix} D\nabla^2 + \nu\Sigma_f(1-\beta) - \Sigma_a & -\nu\Sigma_f\beta \\ \lambda & -u\dfrac{\partial}{\partial z} + \lambda \end{pmatrix} \tag{36}$$

whereas the boundary condition for the adjoint precursors will now read as

$$C_0^{\dagger}(H) = C_0^{\dagger}(0)e^{-\lambda\tau_L} \tag{37}$$

It is easy to prove that with this construction, Eq (35) holds. It is seen that the terms resulting from the off-diagonal and constants elements are equal, only the convection terms need to be checked. Taking the difference between the terms from the two sides of Eq. (35) one has

$$\begin{aligned} & u\int_0^H \left\{ C^{\dagger}(z)\frac{dC(z)}{dz} + C(z)\frac{dC^{\dagger}(z)}{dz}\right\}dz = \left[C(z)C^{\dagger}(z)\right]_{z=0}^{H} \\ & = C(H)C^{\dagger}(H) - C^{\dagger}(0)C(0) = C(H)C^{\dagger}(H) - C(H)e^{\lambda\tau_L}C^{\dagger}(H)e^{-\lambda\tau_L} = 0 \end{aligned} \tag{38}$$

This proves that the adjoint property is fulfilled by the operator (36) and the boundary conditions for the adjoint precursor density (37).

Similarly to what was done for the direct equation (see previous report), the adjoint precursors can be eliminated from the coupled equations by quadrature, and an integro-differential equation can be derived for the adjoint flux alone. The direct equation can be also cast into operator form,

$$\mathbb{L}\phi_0(z) = 0,$$

where

$$\begin{aligned} & \mathbb{L}\phi_0(z) \equiv D\nabla^2\phi_0(z) + \nu\Sigma_f(1-\beta) - \Sigma_a \ \phi_0(z) + \\ & e^{-\frac{z\lambda}{u}}\frac{\lambda\beta\nu\Sigma_f}{u}\left(\frac{1}{e^{\lambda\tau}-1}\int_0^H e^{\frac{z'\lambda}{u}}\phi_0(z)dz' + \int_0^z e^{\frac{\lambda z'}{u}}\phi_0(z')dz'\right). \end{aligned} \tag{39}$$

The derivation of the adjoint equation goes on similar lines, the result being

$$\begin{aligned} & \mathbb{L}^{\dagger}\phi_0^{\dagger}(z) \equiv D\nabla^2\phi_0^{\dagger}(z) + \nu\Sigma_f(1-\beta) - \Sigma_a \ \phi_0^{\dagger}(z) \\ & -e^{\frac{z\lambda}{u}}\frac{\lambda\beta\nu\Sigma_f}{u}\left(\frac{1}{e^{-\lambda\tau}-1}\int_0^H e^{\frac{-z'\lambda}{u}}\phi_0^{\dagger}(z')dz' + \int_0^z e^{\frac{-\lambda z'}{u}}\phi_0^{\dagger}(z')dz'\right) = 0. \end{aligned} \tag{40}$$

The proof of the adjoint property, based on (39) and (40), is a much more complicated task than the previous form on the coupled equations where the flux and precursor densities were kept explicit in both the forward and the backward form.

The proof of the fact that the adjoint operator and adjoint flux indeed fulfil the adjoint property in this form implies that

$$\left\langle \phi_0^\dagger \mid \mathbb{L}\phi_0 \right\rangle = \left\langle \mathbb{L}^\dagger \phi_0^\dagger \mid \phi_0 \right\rangle. \tag{41}$$

The first two terms in the equations, i.e. the Laplace operator and the constant terms, obviously cause no difficulties. It is the last two terms, in the second lines of the equations, which are troublesome. Actually the two terms do not fulfil separately the adjoint property, only together. In order to prove the equality, the following actions are necessary:

- in the third term, the order of integration has to be changed;

$$\int_0^H e^{-\frac{z\lambda}{u}} \phi_0^\dagger(z) \int_0^H e^{\frac{z'\lambda}{u}} \phi_0(z')dz'dz = \int_0^H e^{\frac{z\lambda}{u}} \phi_0(z) \int_0^H e^{-\frac{z'\lambda}{u}} \phi_0^\dagger(z')dz'dz \tag{42}$$

- in the fourth term, the changing of the order of the integrations requires the application of the identities

$$\int_0^H A(z) \int_0^z B(z')dz'dz = \int_0^H B(z) \int_z^H A(z')dz'dz \tag{43}$$

and

$$\int_z^H A(z')dz' = \int_0^H A(z')dz' - \int_0^z A(z')dz' \tag{44}$$

Then one has

$$\begin{aligned}
&\int_0^H \phi_0^\dagger(z) e^{-\frac{z\lambda}{u}} \left(\frac{1}{e^{\lambda\tau}-1} \int_0^H e^{\frac{z'\lambda}{u}} \phi_0(z')dz' + \int_0^z e^{\frac{z'\lambda}{u}} \phi_0(z')dz' \right) = \\
&\int_0^H \phi_0(z) e^{\frac{z\lambda}{u}} \left(\left(\frac{1}{e^{\lambda\tau}-1} + 1 \right) \int_0^H e^{-\frac{z'\lambda}{u}} \phi_0^\dagger(z')dz' - \int_0^z e^{-\frac{z'\lambda}{u}} \phi_0 \delta(z')dz' \right) = \\
&-\int_0^H \phi_0(z) e^{\frac{z\lambda}{u}} \left(\frac{1}{e^{-\lambda\tau}-1} \int_0^H e^{-\frac{z'\lambda}{u}} \phi_0^\dagger \delta(z')dz' + \int_0^z e^{-\frac{z'\lambda}{u}} \phi_0^\dagger \delta(z')dz' \right)
\end{aligned} \tag{45}$$

where in the first equality equations (43) and (44) were used. This proves that Eq. (41) indeed holds.

3.3 The Green's function

In the previous report, two Green's functions were presented: one analytical for infinite fuel velocity, and a numerical solution for finite fuel velocity. The latter of these suffered from some distinct problems: at high frequencies, the truncated series expansion showed some distinctly unphysical behaviour, with undulating space dependence. Increasing the number of terms can make it valid for higher frequencies, but is computationally costly and thus not an attractive solution. Instead, we will present a solution inspired by that of the infinite fuel velocity, where the Greens function was divided into two parts: one which can be seen as a prompt system, and one which

incorporates the effects of the delayed neutrons. The first part will be represented analytically, and the second by a series expansion.

We start with a recapitulation of the original idea: the static flux is represented by a series expansion

$$\phi_0(z) = \sum_{n=1}^{N} a_n \sin B_n z \tag{46}$$

and the Green's function by

$$G(z, z_p, \omega) = \sum_n \bar{a}_n(\omega) \sin B_n z, \tag{47}$$

where $B_n = \frac{n\pi}{H}$. This leads to the following equation

$$\sum_n \left(\left(-DB_n^2 + \nu\Sigma_f(1-\beta) - \Sigma_a - \frac{i\omega}{v} \right) \delta_{mn} + \frac{\beta\nu\Sigma_f}{(H+L)} (\bar{b}_{mn}(\omega) + \bar{c}_{mn}(\omega)) \right) \bar{a}_n(\omega) = \bar{d}_m, \tag{48}$$

where

$$\bar{b}_{mn}(\omega) = \frac{1}{e^{(\lambda+i\omega)\tau_L} - 1} \frac{((-1)^n e^{-\tau_C(\lambda+i\omega)} - 1)((-1)^m e^{\tau_C(\lambda+i\omega)} - 1) B_m B_n}{\left(\left(\frac{\lambda+i\omega}{u} \right)^2 + B_m^2 \right) \left(\left(\frac{\lambda+i\omega}{u} \right)^2 + B_n^2 \right)}, \tag{49}$$

$$\bar{c}_{mn}(\omega) = \begin{cases} \dfrac{(1-(-1)^m e^{-\tau_C(\lambda+i\omega)}) B_m^2}{\left(\left(\frac{\lambda+i\omega}{u} \right)^2 + B_m^2 \right)^2} + \dfrac{\tau_C(\lambda+i\omega)}{2\left(\left(\frac{\lambda+i\omega}{u} \right)^2 + B_m^2 \right)} & n = m \\ \dfrac{B_m B_n \left(-1 + (-1)^{m+n} \left(\frac{\lambda+i\omega}{u} \right)^2 - (-1)^{m+n} B_m^2 + B_n^2 \right)}{\left(\left(\frac{\lambda+i\omega}{u} \right)^2 - B_m^2 \right) \left(\left(\frac{\lambda+i\omega}{u} \right)^2 - B_n^2 \right) B_n^2 - B_m^2} & \\ - \dfrac{B_m B_n \left((-1)^m e^{-i\tau_C(\lambda+i\omega)} \right)}{\left(\left(\frac{\lambda+i\omega}{u} \right)^2 - B_m^2 \right) \left(\left(\frac{\lambda+i\omega}{u} \right)^2 - B_n^2 \right)} & n \neq m \end{cases} \tag{50}$$

and

$$\bar{d}_m = \sin B_m z_p \tag{51}$$

The expansion of the static flux is still valid and will be kept. However, the expansion of the Green's function requires many terms to capture the expected spike-like shape at high frequencies, so we shall try to use the following instead:

$$G(z,z_p,\omega)=G_i(z,z_p,\omega)+G_h(z,z_p,\omega). \tag{52}$$

where

$$G_h(z,z_p,\omega)=\sum_n \bar{a}_n(\omega)\sin B_n z, \tag{53}$$

and $G_i(z,z_p,\omega)$ satisfies

$$D\nabla^2 G_i(z,z_p,\omega)+\left((1-\beta)\nu\Sigma_f-\Sigma_a-\frac{i\omega}{v}\right)G_i(z,z_p,\omega)=\delta(z-z_p). \tag{54}$$

The equations for the delayed neutrons will then be

$$\begin{aligned}
&D\nabla^2 G_h(z,z_p,\omega)+(\nu\Sigma_f(1-\beta)-\Sigma_a-\frac{i\omega}{v})G_h(z,z_p,\omega)+\\
&e^{-\frac{(\lambda+i\omega)z}{u}}\frac{\lambda\beta\nu\Sigma_f}{u}\left(\frac{1}{e^{(\lambda+i\omega)\tau}-1}\int_0^H e^{\frac{(\lambda+i\omega)z'}{u}}G_h(z',z_p,\omega)dz'+\int_0^z e^{\frac{(\lambda+i\omega)z'}{u}}G_h(z',z_p,\omega)dz'\right)=\\
&-e^{-\frac{(\lambda+i\omega)z}{u}}\frac{\lambda\beta\nu\Sigma_f}{u}\left(\frac{1}{e^{(\lambda+i\omega)\tau}-1}\int_0^H e^{\frac{(\lambda+i\omega)z'}{u}}G_i(z',z_p,\omega)dz'+\int_0^z e^{\frac{(\lambda+i\omega)z'}{u}}G_i(z',z_p,\omega)dz'\right)
\end{aligned} \tag{55}$$

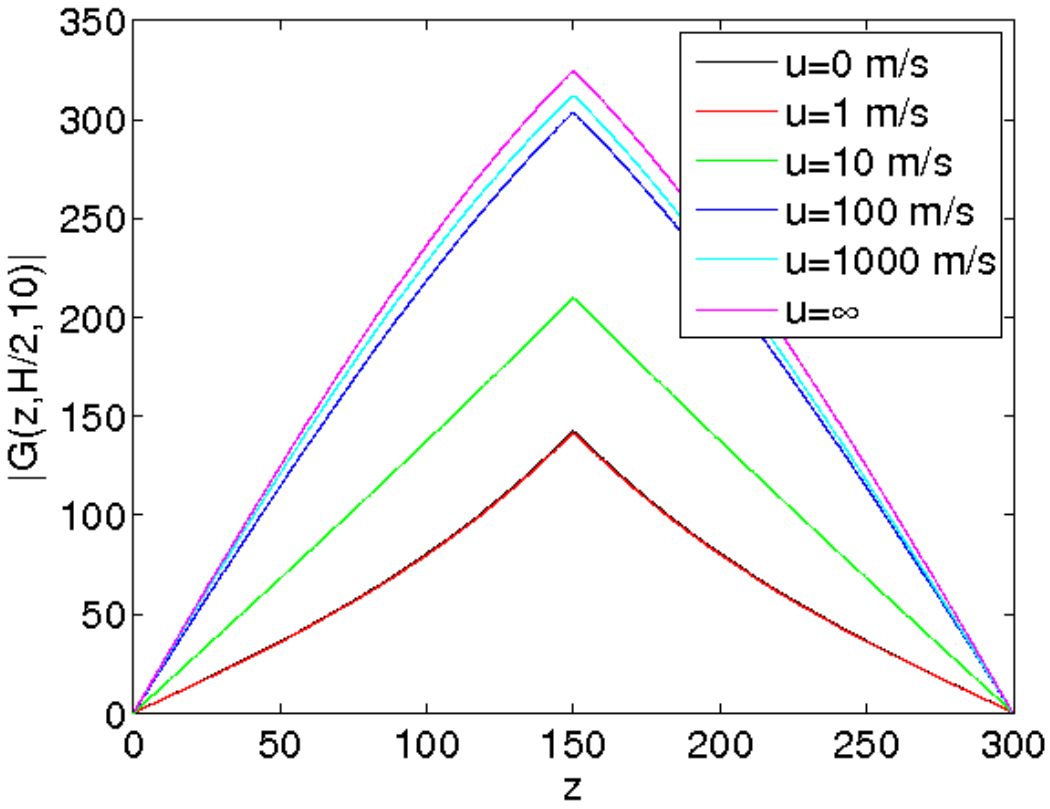

Fig. 16. Green's function space dependence for some different velocities. Analytical solution for $u = 0$ *and* $u = \infty$. $H = 300$ *cm,* $\omega = 10$ *rad/s.*

The left hand side of this equation is the same as that of the original equation for $G(z, z_p, \omega)$, only the right hand side changed from the Dirac delta to a smooth function. This shows the analogy with the solution of the transport equation with eliminating the singular uncollided flux and solving an equation for the much smoother flux of collided particles. This means also that the matrix equation for the expansion coefficients $\bar{a}_n(\omega)$ will have the same form as (48)- (50), while the expression for $\bar{d}_m$ will be substantially more involved. However, the solution goes the same way by inverting the matrix on the l.h.s.

Numerical results are shown in Figs 15 and 16.

Fig. 15 shows the frequency dependence of the amplitude of the Green's function in the smaller system for various fuel velocities. At the lowest velocity, the frequency dependence is the same as that of the amplitude of the zero power transfer function $G_0(\omega)$: a plateau at medium frequencies, and an $1/\omega$ behaviour at low and high frequencies. At higher frequencies, some multiple ripples appear. The frequencies where these appear correspond to the inverse of the recirculation time of the fuel. With higher velocities, these appear at higher frequencies.

Fig. 16 shows the space dependence of the amplitude of the Green's function in the large system, for $z_0 = H/2$ and a frequency of $\omega = 10$ rad/s, which is in the middle of the plateau region, for a few different velocities. For $u = 0$, that is a traditional reactor, the Green's function is relatively localised and indicates substantial deviation from the point kinetic behaviour. For increasing fuel velocities, partly the amplitude of the Green's function increases, and partly its shape is changed towards a more point-kinetic type behaviour. The reasons of these effects were already touched upon; the increase of the amplitude is due to the loss of neutrons decaying from precursors outside the core, and the point kinetic behaviour is due to the increased neutronic coupling between various parts of the core, due to the fuel flow and the movement of the precursors.

3.4 Propagating perturbations

In traditional light water reactors, the propagation of the coolant, through its non-completely homogeneous structure, represents a perturbation which has the property of propagating through the core. In pressurized water reactors (PWRs), the small fluctuations of the inlet temperature, affecting e.g. the absorption cross sections, represents a propagating perturbation whose effect on the neutron flux can be measured. Such propagating perturbations and their effect on the neutron noise were studied before (Kosály, 1971; Kosály, 1972, Wach, 1974) as well as recently (Dykin, 2010). In the earlier works, the neutron noise was only calculated in the point kinetic approximation. The space dependence was calculated only very recently (Dykin, 2010). This interest was clearly triggered by the renewed interest in Molten Salt Reactors, in which such perturbations will be present in a stronger from than in a PWR, since it will be the properties of the propagating fuel that will have some random variations in contrast to those of the coolant in a PWR. However, the neutronic response of the MSR will also be different, as we have already seen at the level of the Green's function. So the space-dependent neutron noise due to propagating perturbations is interesting both in traditional reactors and in the MSR.
The propagating perturbation can be represented as

$$\delta\Sigma_a(z,t) = \delta\Sigma_a(0, t - z/u) \tag{56}$$

and thus in the frequency domain one has

$$\delta\Sigma_a(z,\omega) = e^{\frac{-i\omega z}{u}} \delta\Sigma_a(0,\omega). \tag{57}$$

Here the process $\delta\Sigma_a(z=0,t)$, i.e. the perturbation at the inlet of the core, is usually considered as a white noise process, so the frequency dependence of its autospectrum is constant. This is often represented such that $\delta\Sigma_a(0,\omega)$ is taken as a constant, although strictly speaking it is only valid for its autospectrum. This latter is, however, calculated by the Wiener-Khinchin theorem as its own absolute value squared, so the assumption of $\delta\Sigma_a(0,\omega)$ being constant does not lead to any contradictions. Hence in the continuation we set $\delta\Sigma_a(0,\omega) = 1$.

As is known (Kosály, 1972) the reactivity effect of such a perturbation, calculated as

$$\rho(\omega) = -\frac{\int \phi_0^2(z)\delta\Sigma_a(z,\omega)dz}{\nu\Sigma_f \int \phi_0^2(z)dz} \tag{58}$$

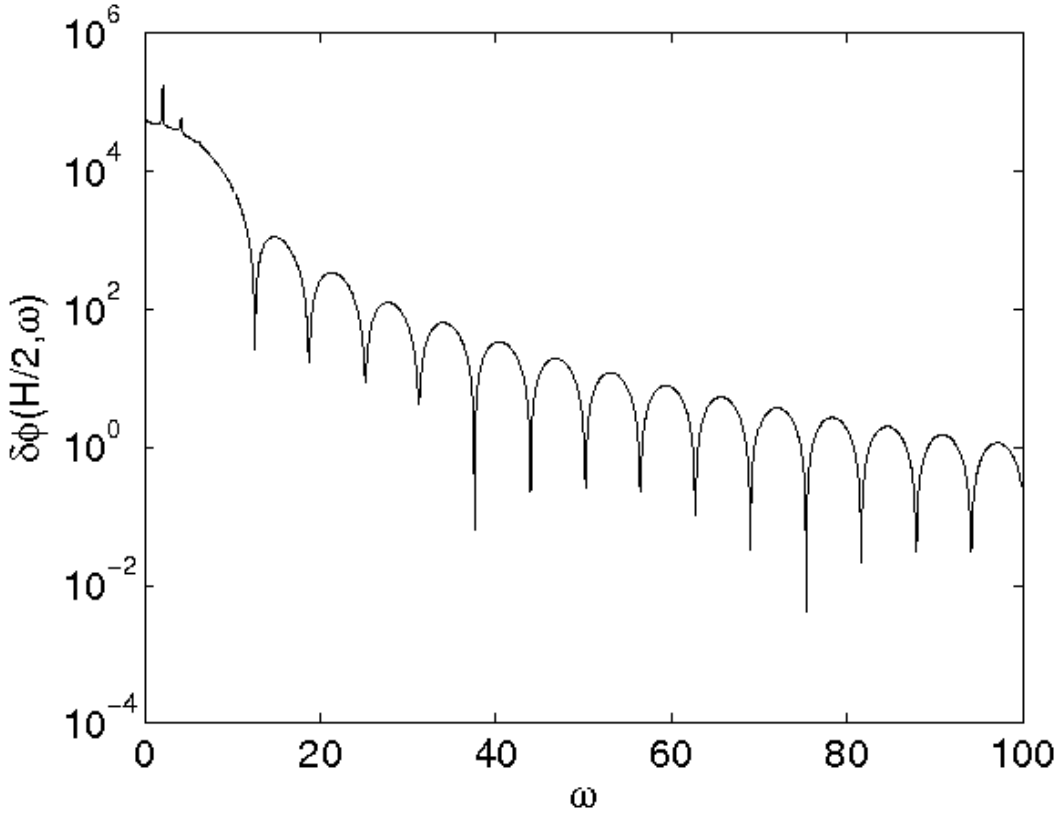

Fig. 17. The frequency dependence of the neutron noise induced by a propagating perturbation in a small system (H =50 cm)

shows a characteristic, periodic sink structure, i.e. it has zeros (``sinks") at

$$\omega = \frac{2\pi u}{H} n = \frac{2\pi}{\tau_c} n; \qquad n = 2,3\ldots \tag{59}$$

where τ_c is the transit time of the fuel (coolant) through the core. This sink structure of the reactivity, which immediately affects the frequency dependence of the induced neutron noise, especially in the case of point kinetic behaviour, will be used to interpret the results from the space dependent calculations.

The space dependent noise can be calculated by the help of the Green's function, which we determined earlier. The noise is then given as

$$\delta\phi(z,\omega) = \int_{-a}^{a} G(z,z_0,\omega) e^{\frac{-i\omega z_0}{u}} \phi_0(z_0) dz_0 \tag{60}$$

A few characteristic results will be shown for illustration.

The frequency dependence of the noise in a small system is shown in Fig. 17 as measured in the centre of the system. Such a small system is assumed to behave in a point kinetic manner up to high frequencies (especially in the MSR which, as it was noticed, behaves more point kinetically as a corresponding traditional system). Hence the resulting noise shows the sink structure of the reactivity, modulated by the frequency dependence of the transfer function, which is seen in Fig. 15. Also the ripples at low

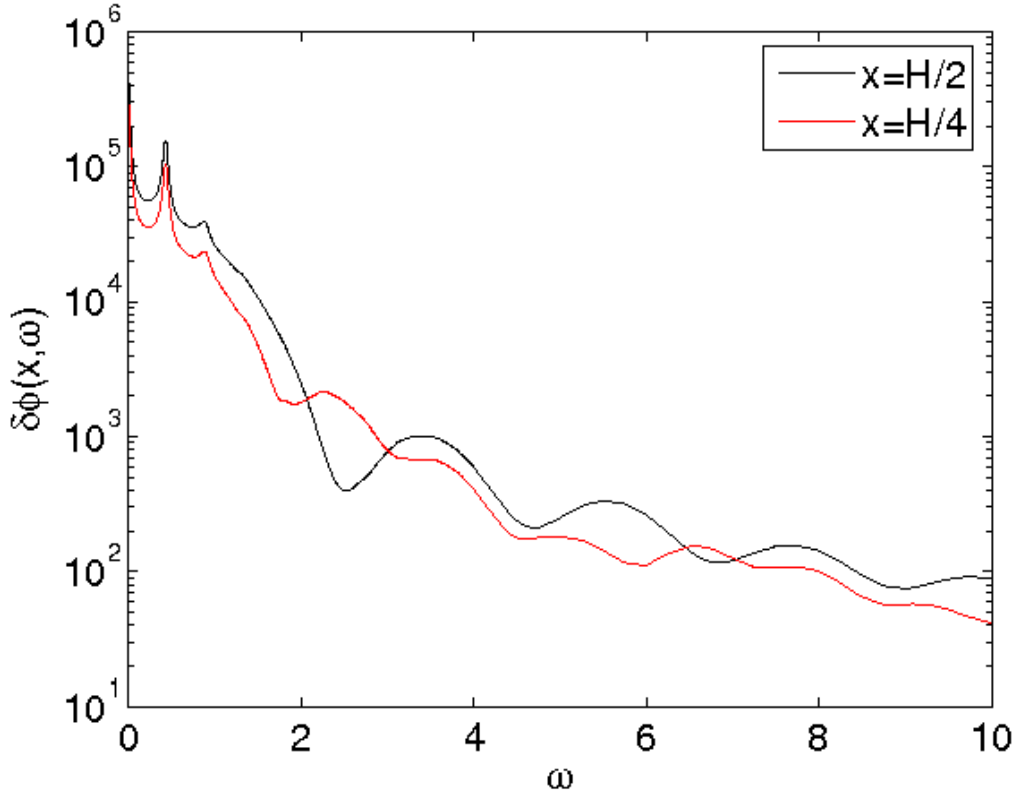

Fig. 18. The frequency dependence of the neutron noise induced by a propagating perturbation in two different points in a large system (H =300 cm).

frequency can be seen, although less visibly, due to the linear plot in the x-axis in this figure. For the large system (Fig. 18), the situation is rather different. At low frequencies, the ripples due to the fuel recirculation are still visible. However, the sink structure at higher frequencies is rather different and less marked. Moreover, the frequency dependence is different in different parts of the reactor, as is seen in the figure which shows the noise in two different points of the reactor.

The diminishing of the sink structure is largely due to the less dominant contribution from the point kinetic components, since it is only this component which has the sink structure. The further deviations below the plateau frequencies can be partly understood from the interference between the point kinetic and space dependent components of the induced noise, as it was discussed in a companion paper, dealing with the space-dependent effect of propagating perturbations in traditional reactors (Dykin, 2010). This interference arises from the fact that the point kinetic component has a uniform phase across the whole core, whereas the phase of the space dependent term follows that of the perturbation. As seen from (57), the phase of the latter is

$$\varphi = \frac{\omega}{u} z,$$

i.e. it changes linearly with the position in the core. Hence the two components are in certain points in-phase, at some other point out-of-phase, leading to constructive and destructive interference, respectively. The result is the somewhat complicated frequency behaviour seen in Fig. 18.

Further insight can be gained by investigating the space dependence of the noise for different frequencies. We show this space dependence in the large system at two different frequencies. In Fig. 19 the space dependence is shown for low and medium frequencies. At low frequencies, the system behaves in a point kinetic manner; hence the amplitude of the noise follows the shape of the static flux.

At the higher frequency of $\omega = 10$ rad/s, which is in the middle of the plateau region, the space dependence suddenly shows local maxima and minima, although the space dependence of both the point kinetic and the space-dependent parts is smooth and similar to the static flux. As it was mentioned before and is discussed in detail in (Dykin, 2010), the maxima correspond to the core positions where the point kinetic and space dependent terms are in-phase, and the local minima to the points where they are out of phase. The reason that no such non-monotonic behaviour is seen at low frequency is partly that at lower frequency the spatial oscillations of the phase of the space-dependent term are much slower and more important, the point kinetic component dominates and hence the interference has no effect. At the plateau frequency, the point kinetic component has decreased such that the two components are comparable in amplitude. This is why the spatially oscillatory behaviour of the noise is so marked. At even higher frequencies, the point kinetic term decreases further, and the spatial behaviour becomes smooth again, because it is dominated by the space-dependent component alone.

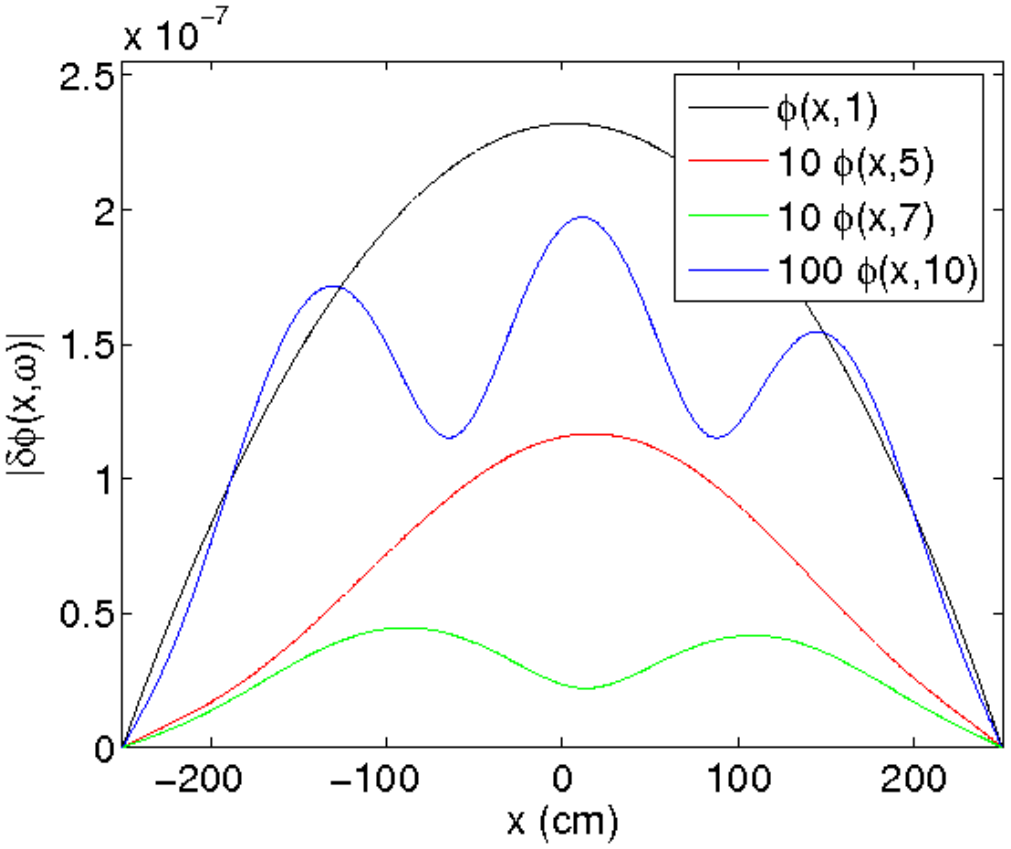

Fig. 19. Comparison between the neutron noice space dependence for different frequencies in a large system ($H = 500$ cm, $v = 250$ cm/s).

It is also interesting to make a comparison with traditional systems. As is shown in (Dykin, 2010), in a traditional system of the same size, at the plateau frequency, the noise is dominated by the space-dependent component, hence the interference and the spatially oscillatory behaviour of the noise is largely absent. It can only be observed at much lower frequencies in the large system. The fact that this interference of the two components exists at plateau frequencies in an MSR is a further indication of the fact that an MSR behaves in a more point kinetic manner than a corresponding traditional system.

4 A specific study of the novel methods of analysis of non-linear and non-stationary processes

4.1 Introduction

This section gives a brief overview of the first, preliminary results obtained with the application of some new data analysis techniques to neutron noise measurements, such as peak-to-peak interval analysis, as well as Principal Component Analysis (PCA) and Singular Value Decomposition (SVD). These methods are supposed to be suitable for the analysis of non-linear and non-stationary processes, and we chose the analysis of BWR stability measurements, as one application. The measurements analysed were taken under different operational conditions, i.e. at two different operational points on the power-flow map. The chosen operational points contain one stable and one unstable point. One long-term objective of the investigations is to see whether application of these methods might lead to the development of new indicators to the margin to instability. However, in this first pilot study, the ambition is clearly lower, and is restricted to a comparison of the results of the peak-to-peak, PCA and SVD analysis of data corresponding to a stable and an unstable point, to see if one can find any qualitative and quantitative differences between the two cases.

These techniques are not applied directly to the time series signals, rather to a derived quantity, which was also used in connection with other quasi-periodic and non-stationary signals, such as heart rate analysis. Namely, the time series to be analysed is the sequence of peak-to-peak time intervals, where the peaks correspond to the maxima (or minima) of the quasi-periodic part of the signal, represented by the unstable oscillations. Unlike in the case of heart beat signals where the peaks are very visible directly in the time series signal, in case of in-core neutron signals, the large energy low-frequency component of the signal usually covers and hides the quasi-periodic oscillations around 0.5 Hz. Hence the extraction of the peak-to-peak time intervals is an interesting first task to be solved.

4.2 Principles

The principles of the method of applying peak-to-peak analysis with a direct visual way, without further algorithmic processing, are described in an article by Morfill and Bunk (2001). The method is also illustrated in Fig. 20. The time intervals between the maxima of the ECG signal, denoted in the Figure as RR_i with *i* being the sequential number, are taken as digitized samples of a signal. Plotting such a time series, as will be seen later on in our calculations, behaves like a true random process without visible strong periodic components. Such a time series carries important diagnostic information about the system, which can be unfolded in many ways. The one used in the work by Morfill and Bunk (2001) is based on constructing three-dimensional vectors from three consecutive values of the RR sequence, i.e. $V_1 = \{RR_1, RR_2, RR_3\}$, $V_2 = \{RR_2, RR_3, RR_4\}$, etc., and investigate the topological properties of the data set $\{V_i\}$, $i = 1,2....$ As is shown in the article and is illustrated in Fig. 20, such a vector

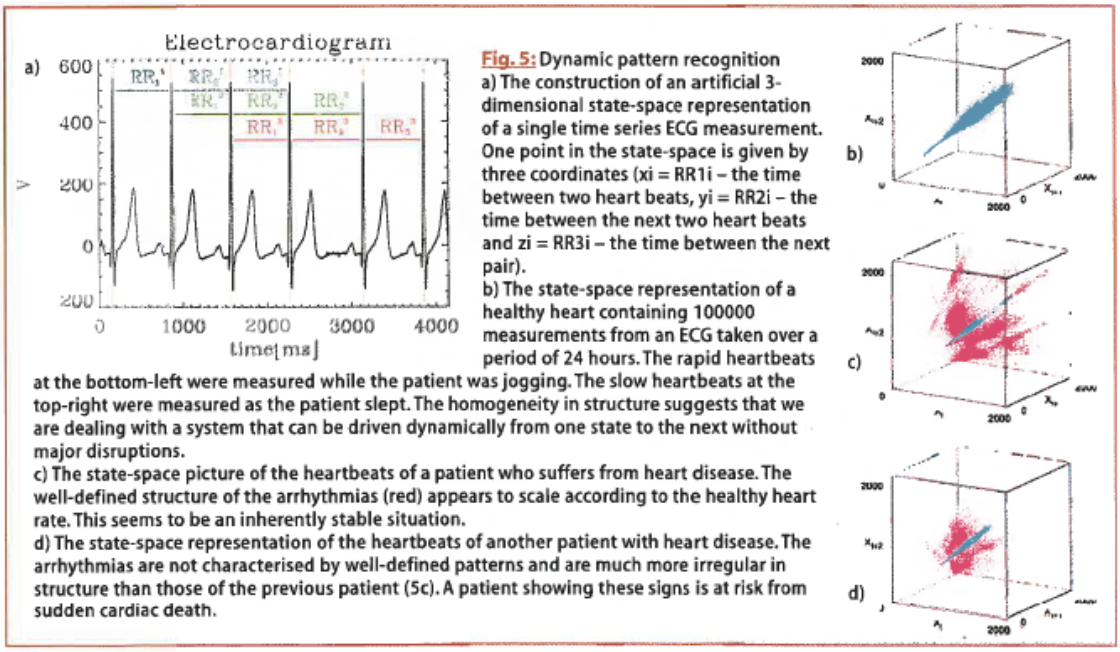

Fig. 5: Dynamic pattern recognition
a) The construction of an artificial 3-dimensional state-space representation of a single time series ECG measurement. One point in the state-space is given by three coordinates (xi = RR1i – the time between two heart beats, yi = RR2i – the time between the next two heart beats and zi = RR3i – the time between the next pair).
b) The state-space representation of a healthy heart containing 100000 measurements from an ECG taken over a period of 24 hours. The rapid heartbeats at the bottom-left were measured while the patient was jogging. The slow heartbeats at the top-right were measured as the patient slept. The homogeneity in structure suggests that we are dealing with a system that can be driven dynamically from one state to the next without major disruptions.
c) The state-space picture of the heartbeats of a patient who suffers from heart disease. The well-defined structure of the arrhythmias (red) appears to scale according to the healthy heart rate. This seems to be an inherently stable situation.
d) The state-space representation of the heartbeats of another patient with heart disease. The arrhythmias are not characterised by well-defined patterns and are much more irregular in structure than those of the previous patient (5c). A patient showing these signs is at risk from sudden cardiac death.

Fig. 20. Principles of peak-to-peak time series analysis for heartbeat signals.

data set has very different properties for healthy persons and for persons with a certain type of heart disease.

This is the method whose application will be attempted to BWR data to explore its potentials for BWR stability characterization. The long-term purpose is finding a new potential stability indicator. There have already been attempts by others to use the same method, but the details are not published, for commercial reasons.

In the quantitative work, the measurement data taken from cycle 14 of Ringhals-1 in 1991 were used. As it is known, in these measurements both global and regional oscillations occurred simultaneously, and in measurement point *G*, a full instability was developed.

4.3 Peak-to-peak time interval analysis of BWR in-core neutron noise signals

BWR in-core neutron noise signals differ significantly from the quasi-periodic character of ECG signals seen in Fig. 20. Except for fully developed instabilities, the oscillation at around 0.5 Hz is masked by a large energy low frequency background. The idea is to use the information in the maxima and/or minima of this 0.5 Hz oscillation to construct the peak-to-peak series. This is a relatively straightforward task for the strongly quasi-periodic ECG signals, but in the case of BWR signal, first the quasi-periodic component has us, our first step is to identify the time-positions of the maxima and minima.

The first step is a bandpass filtering of the initial measurement signal, such that the bandpass filter is centred on the 0.5 Hz oscillation. This can be achieved by digital filtering techniques. Bandpass filters with a frequency band 0.1 – 1 Hz, as well as 0.45 –

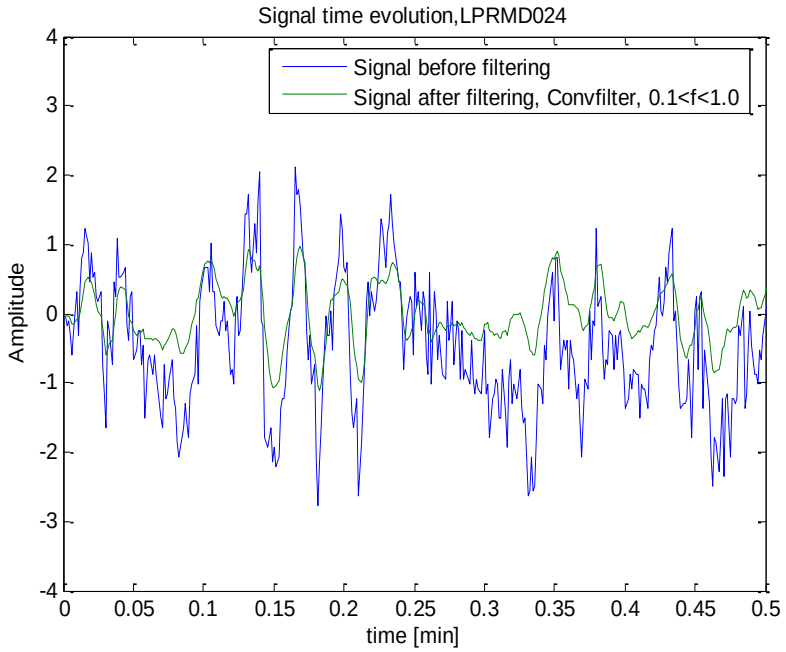

Fig. 21. Raw and filtered signals in the operational point D from LPRM 024.

0.6 Hz were used. The comparison between the unfiltered and filtered signals with the wider bandpass filter is shown in Figs. 21 and 22 for two radial positions in the reactor core. The signals were taken in the stable operational point *D* from the detectors LPRM-024 and LPRM-104.

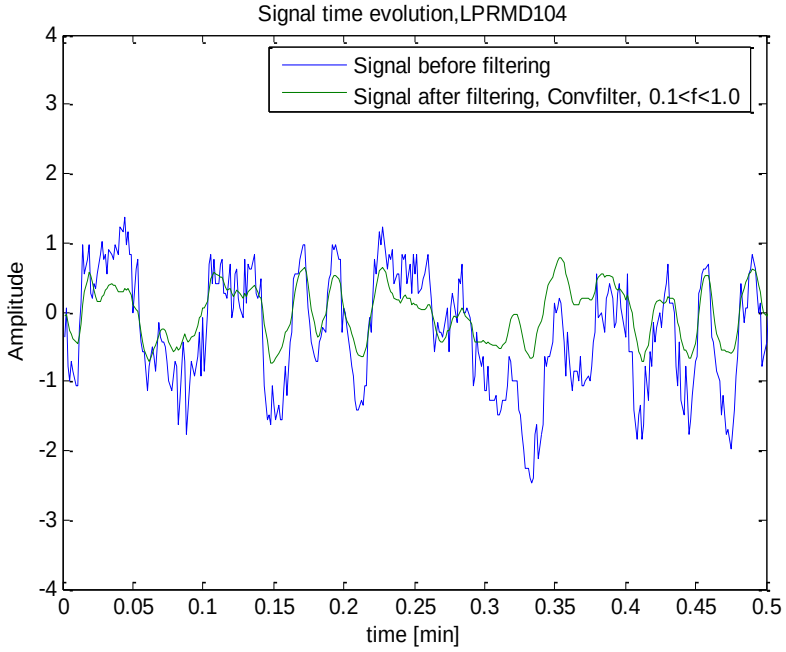

Fig. 22. Raw and filtered signals in the operational point D from LPRM 104.

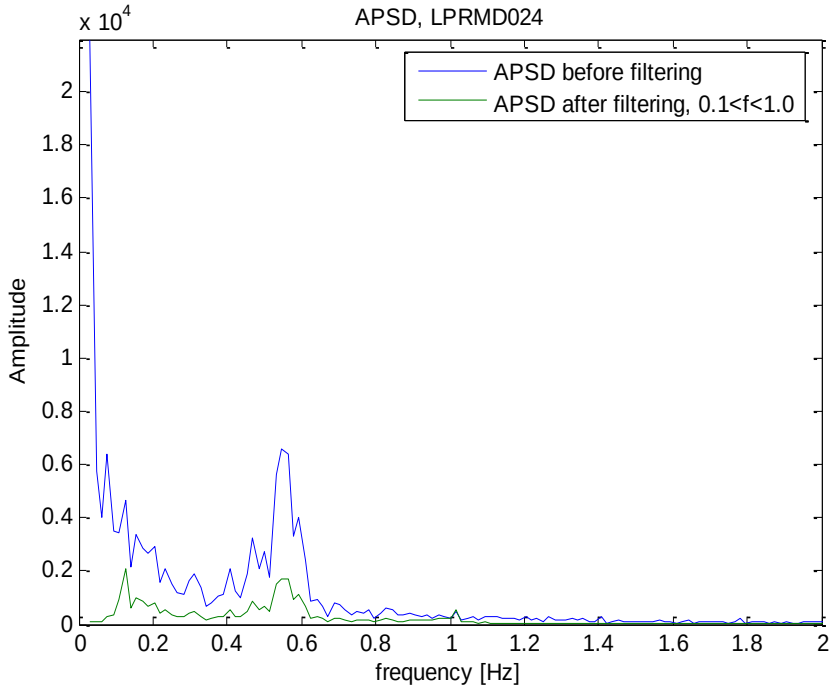

Fig. 23. APSDs of the raw and the filtered signals in the operational point D from LPRM 024

In Figs. 23 and 24 the APSDs of the filtered and unfiltered signals are shown. They show how the large amplitude low frequency part of the spectra is eliminated by the filtering.

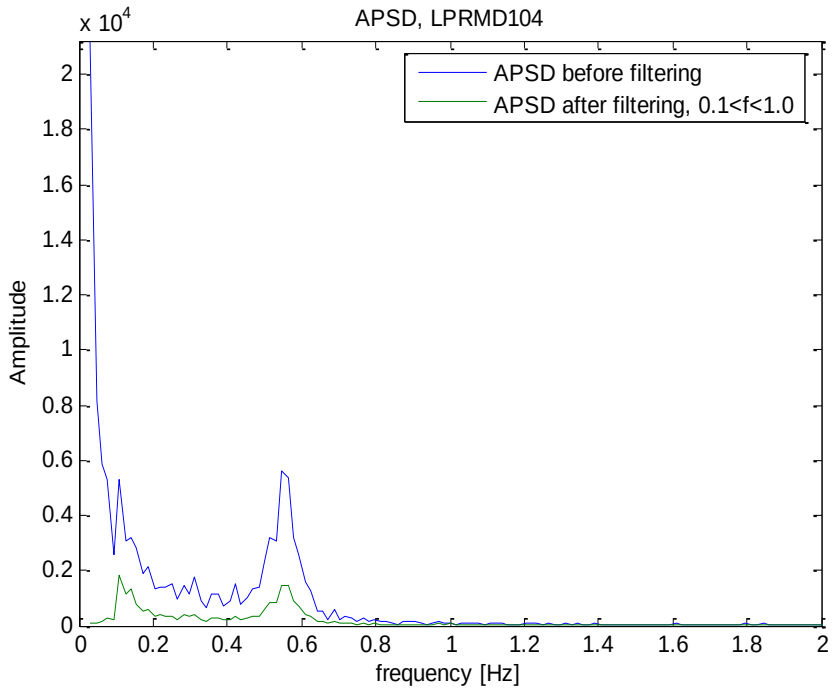

Fig. 24. APSDs of the raw and the filtered signals in the operational point D from LPRM 104

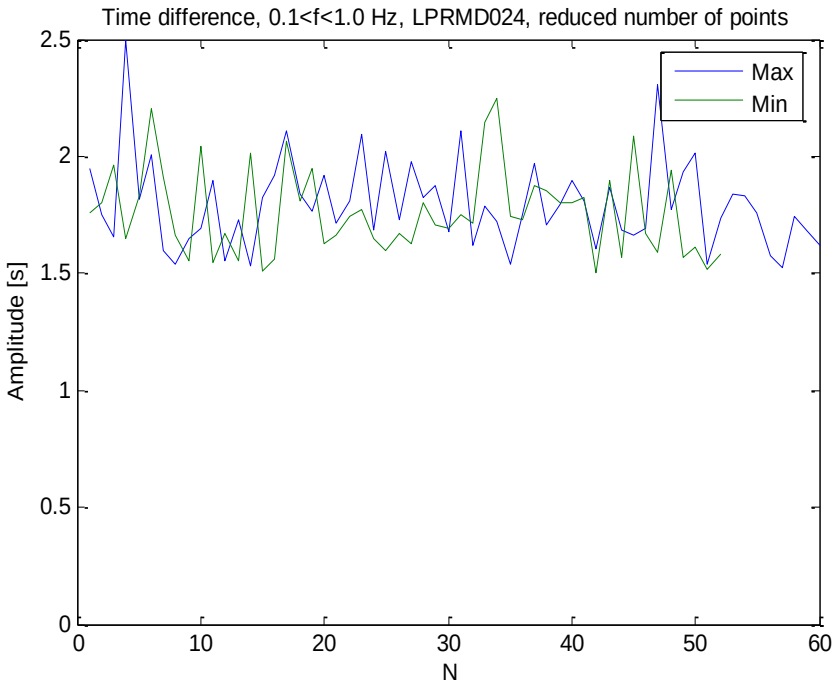

Fig. 25. The peak-to-peak time series for LPRM 024 in operational point D

The next step is to extract the time instants of the minima and maxima of the filtered signal. Here, various methods were tested, such as the sign change of the derivative of the signal, or finding local maxima and minima etc. Some results are shown in Figs. 25 and 26. Since the oscillation frequency is 0.5 Hz, the mean value of the peak-to-peak signals between the maxima or the minima is 2 sec. As one can see the distance between two consecutive minima as well as two consecutive maxima varies around the mean

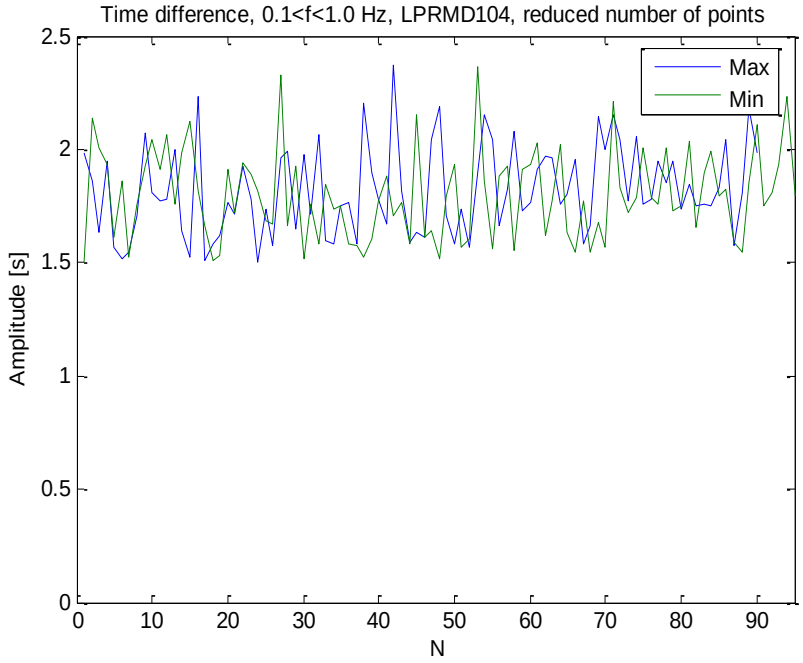

Fig. 26. The peak-to-peak time series for LPRM 104 in operational point D

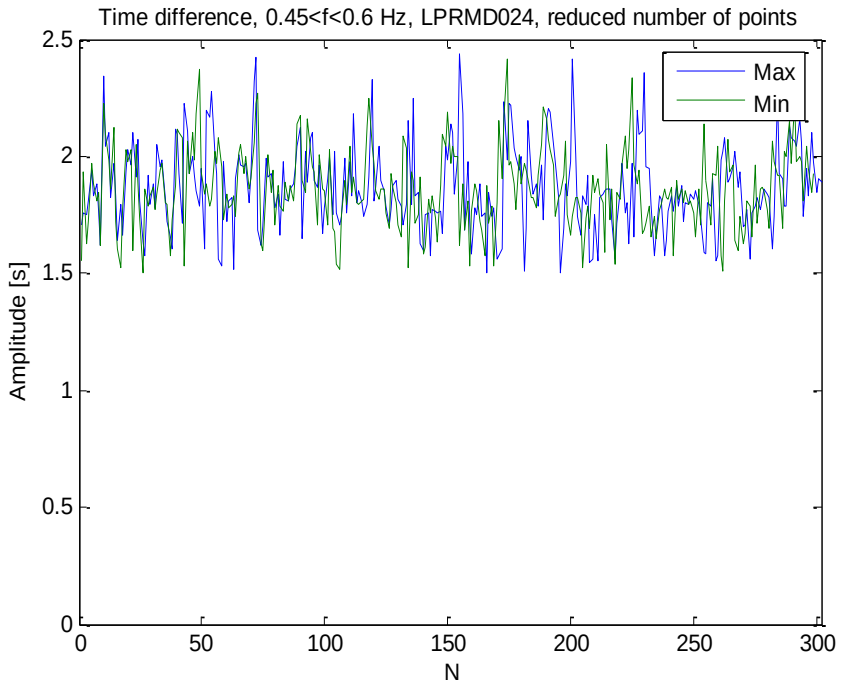

Fig. 27. The peak-to-peak time series for LPRM 024 in operational point D, with a narrow band-pass filter.

value of 2. Fig. 27 shows the result when the filtering was performed with 0.45<f<0.6 Hz. The reduction of the filter bandwidth reduces the amplitude of variations around the mean value but does not change the distribution structure significantly. As expected, the peak-to-peak signals show a random behaviour.

It is now interesting to compare the peak-to-peak sequences for two different operational points: one for the more stable point D and for the unstable point G. The time series sequences are shown in Figs. 25 and 28, respectively, for the same detector. It is seen that the variation of the peak-to-peak series is significantly larger for the stable point than for the unstable one. This corresponds to the fact that the signal is much more periodic (the peak of the APSD much narrower) for the unstable signal than for the stable one.

Next, we construct the set of three-dimensional vectors from the peak-to-peak interval series, as described in the previous section. A 3-D plot of these vector sets is shown in Figs. 29 and 30 for the measurements in the operational points D and G, respectively. In both cases, the data points constitute one data cluster, centred around the diagonal component {2,2,2}.

As one can see from these figures, the behaviour of the 3D measurement points reflects what was already seen on the peak-to-peak time series, Figs. 25 and 28. Namely, the spread of the data is larger for the more stable point *D* than for the unstable point *G*. Beyond that, no further structure, such as sub-clustering, can be seen in any of the vector sets, and the information contained seems to be limited to what can already be determined by the conventional methods. However, so far this is a very preliminary

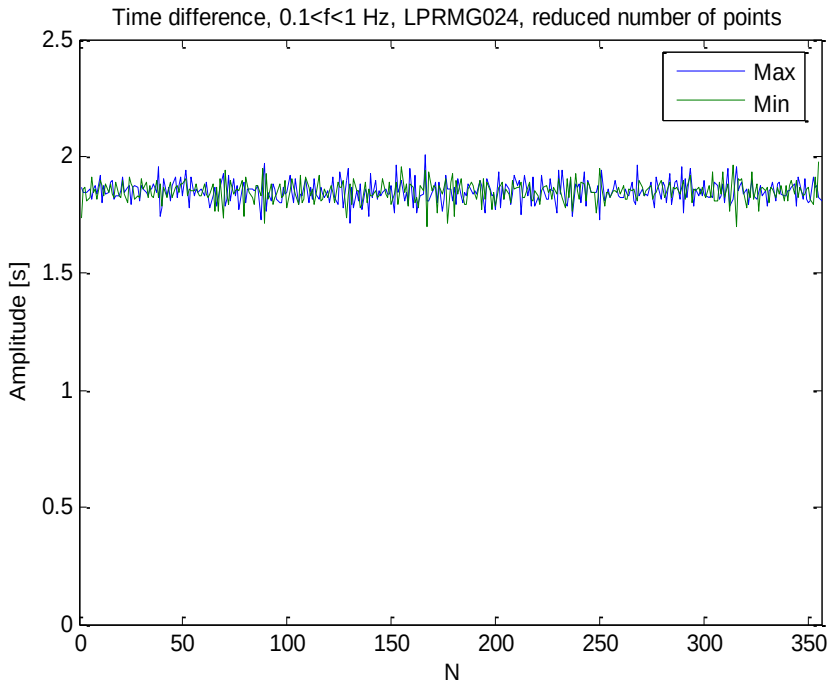

Fig. 28. The peak-to-peak time series for LPRM 024 in operational point G.

analysis, based on a limited data set. Further investigations, with a larger data base, and possibly with the use of higher dimensional vectors will be pursued in the continuation.

4.4 Principal Component Analysis and Singular Value Decomposition

It has been planned already in previous Stages to apply Principal Component Analysis (PCA) and Singular Value Decomposition (SVD) in noise diagnostics. Both methods are based on the reduction of the dimension of the measurement data, which helps to separate the valuable data from the redundant ones and to reveal the hidden structure of the data. The potential benefit of these methods would be if after such a reduction, performed for both the stable and the unstable points, one could correlate the stability properties to the data structure.

The basic idea of the PCA is to find an orthogonal basis through a transformation of the measurement data, such that unnecessary information and redundancy are eliminated. One can illustrate this concept with the following example. A classification of a 2-D random motion of an object (such as the core-barrel, or a vibrating control rod or fuel assembly) can be characterized by the auto- and cross correlations between the *x* and *y* components of the motion (or the APSD and CPSD of the vibration components). Assume now that for a 2-D random motion, the displacements in the *x* and *y* directions are uncorrelated, but with different amplitudes (the APSDs have different magnitudes at the vibration frequency). In such a case the 2-D motion is not isotropic, and the axes of the co-ordinate system in which the motion is observed, coincide with the principal axes of the motion. It is easy to show that, describing the same motion in another coordinate system which is obtained from the original with a rotation which is not equal to 90 degrees or its multiples, then the x and *y* components in the new system become correlated. This is because due to the rotation, the new coordinates will be a linear

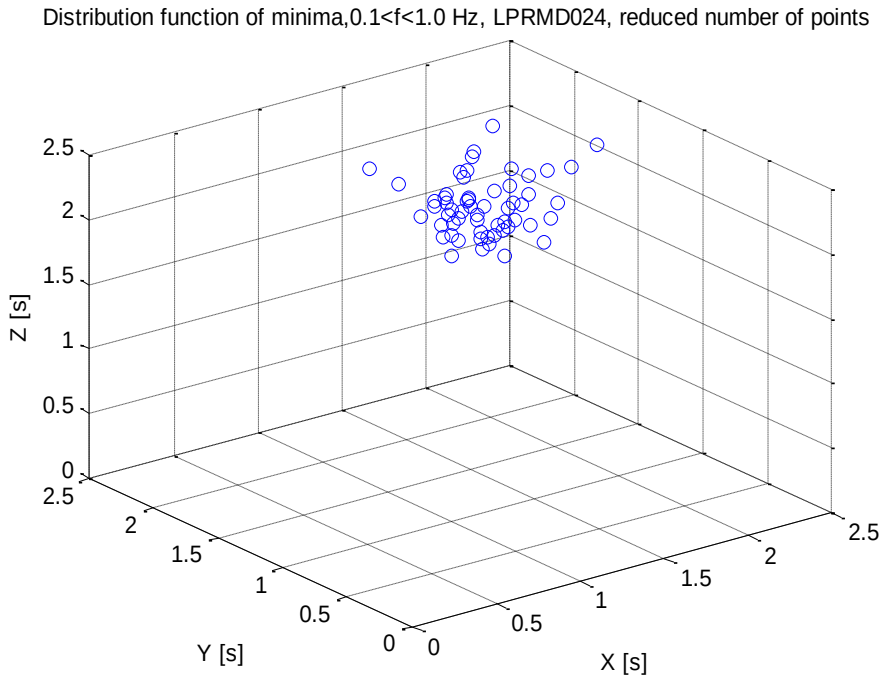

Fig. 29. Plot of the 3-D data vectors, constructed from the peak-to-peak series for measurement D.

combination of the old components. Hence the cross-correlation of the new components will contain auto-correlations of the old components, which are not zero. Since in a measurement one cannot grant that the observation system coincides with the principal axes of the motion, generally there will be a non-zero cross-correlation between the two components. It is important to know whether these correlations are only due to the "mixing" of otherwise uncorrelated components of the motion due to non-optimum choice of the observation system, or indeed there is a physical correlation between the vibration components irrespective of the choice of the coordinate system. A search for a transformation that eliminates the cross-correlation, which is the essence of the PCA, can give the answer.

In order to perform PCA, firstly one needs to transform the measurement data into a vector/matrix form where the column number corresponds to the experimental trial (the measurement number) and the row number corresponds to the measurement type. In our case, the matrix will be constructed such that the rows are given by the 3-D vectors of the peak-to-peak time interval values, and the row number is the sequential number of the vector.

The next step is to construct the covariance matrix from these measurement data. The non-diagonal elements of the covariance matrix are minimized by finding a new basis. In the new basis the covariance matrix should have a different form, such that the non-diagonal elements are minimized and the diagonal ones maximized. After the transformation one obtains the set of independent components of the measurement data or the most important ones, as well as the information about the importance of each component (diagonal components of the covariance matrix.). From linear algebra, it is known that the searched basis can be constructed from the eigenvectors of the

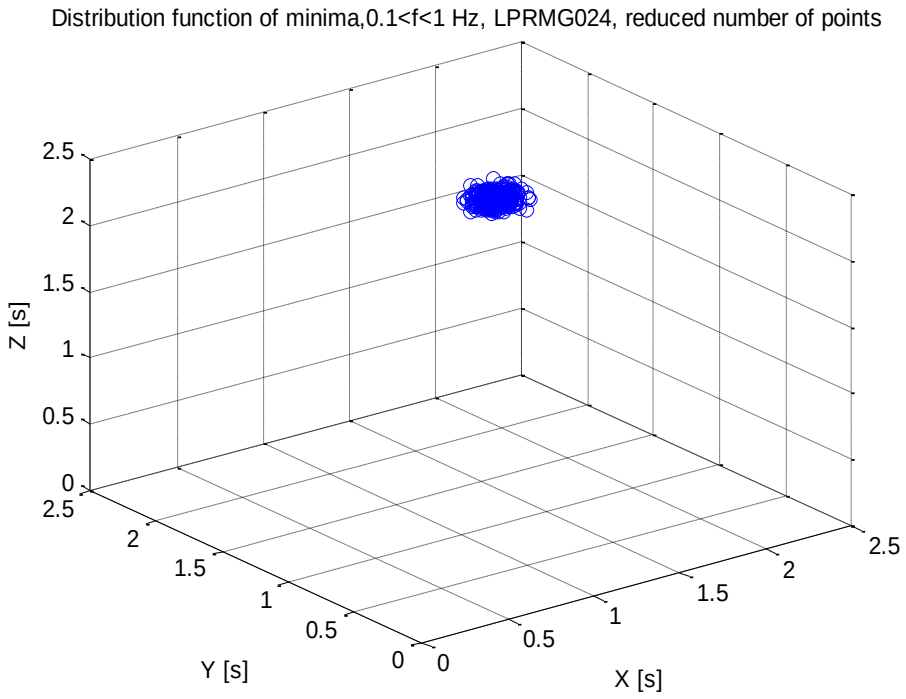

Fig. 30. Plot of the 3-D data vectors, constructed from the peak-to-peak series for measurement G.

covariance matrix. The matrix can be transformed into the diagonal form with the eigenvalues on its main diagonal. In the following considerations, this method is simply denoted as traditional "PCA method".

Another way to perform such analysis is first to use the so-called Singular Value Decomposition (SVD) method and then apply the PCA. The SVD technique allows one to decompose the square matrix into three matrices in such a way that the consecutive multiplication of these matrices yields the initial matrix. The advantage of this method is that it allows to transform the initial matrix into diagonal. Further, this method is referred as "SVD method".

We have applied the PCA method without and with SVD, on a data matrix composed from the 3-D vector sets arranged into a matrix. Existing MATLAB software was used for the purpose. The mean value was previously subtracted from the original data. The application of both "traditional" PCA and the one with SVD transformed the original 3-D data sets, shown in Figs. 29 and 30, into a new data set. The results are shown in Figs. 31 - 35, also including the stable point *H*. There is no significant difference in the data sets before and after the application of both PCA methods what regards the dimensionality of the data vectors, either for the stable or for the unstable point. However, what regards the data values themselves, the traditional PCA and the one with SVD application yield the same results for the stable points, but yield values with much less spread in the unstable point. It will be investigated whether such a difference could be used as a sufficiently sensitive indicator of the development of instability.

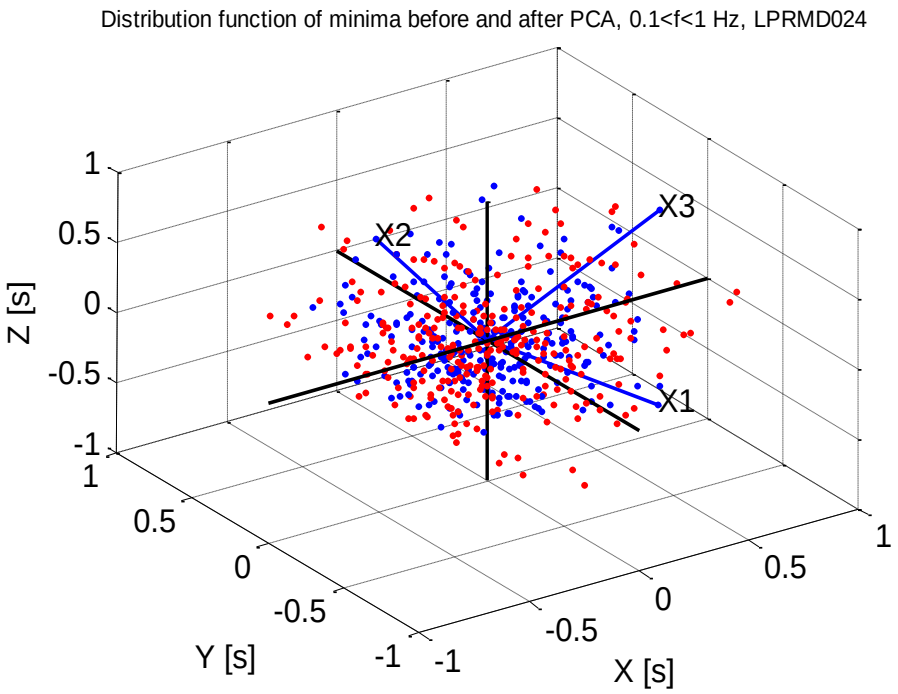

Fig. 31. Distribution of the vector points for LPRM 024 in operational point D, before (blue points) and after (red points) the application of PCA.

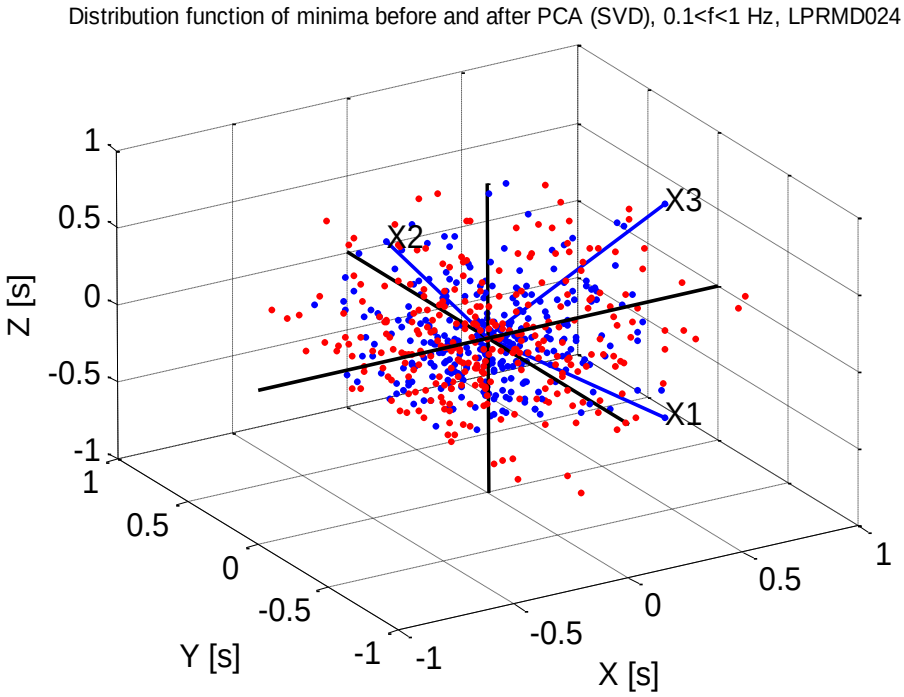

Fig. 32. Distribution of the vector points for LPRM 024 in operational point D, before (blue points) and after (red points) the application of PCA (SVD method).

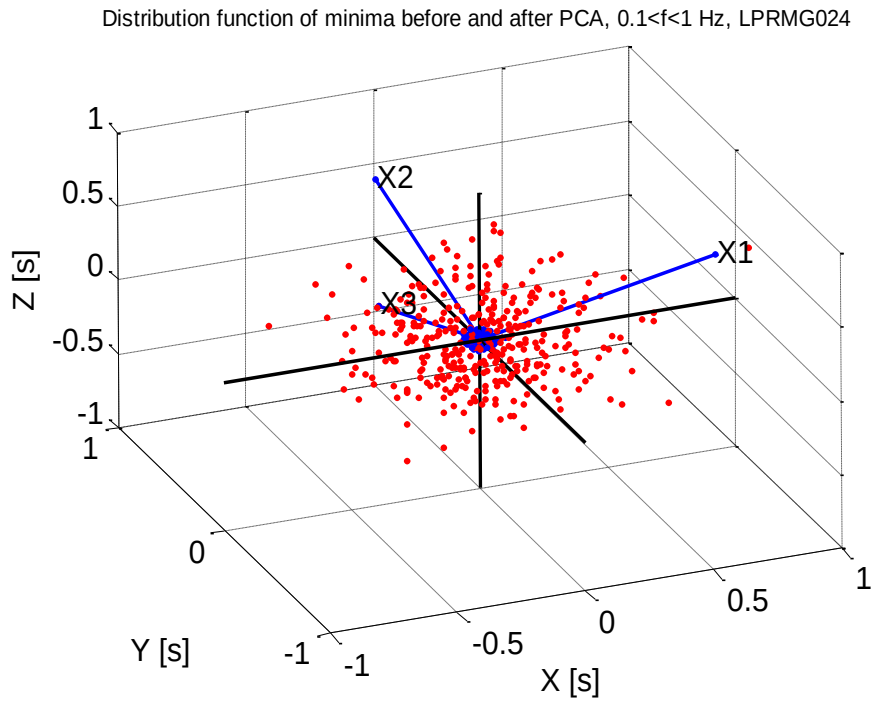

Fig. 33. Distribution of the vector points for LPRM 024 in operational point G, before (blue points) and after (red points) the application of PCA.

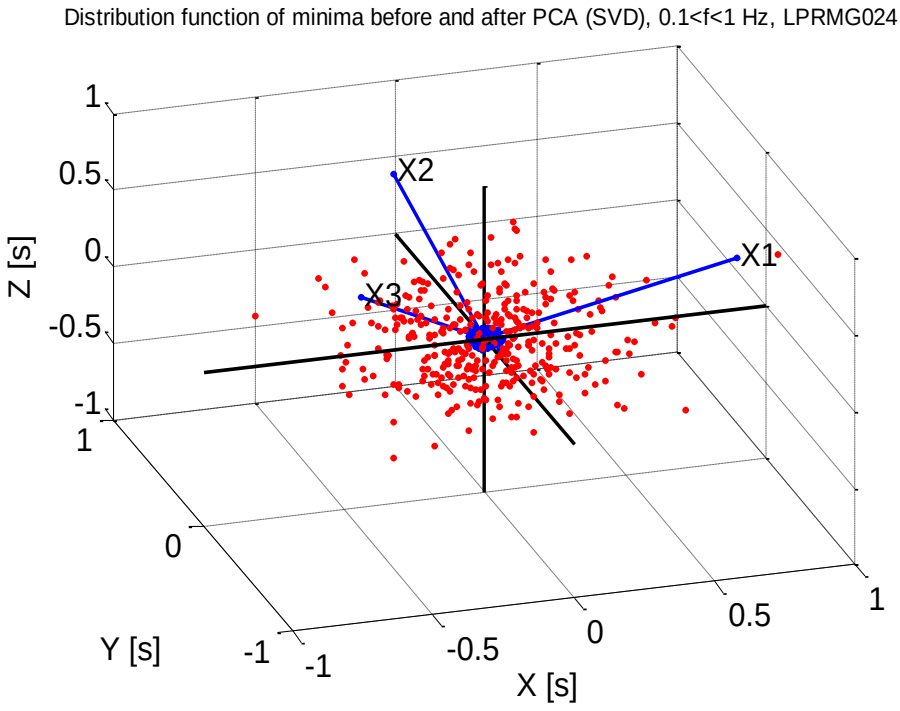

Fig. 34. Distribution of the vector points for LPRM 024 in operational point G, before (blue points) and after (red points) the application of PCA (SVD method).

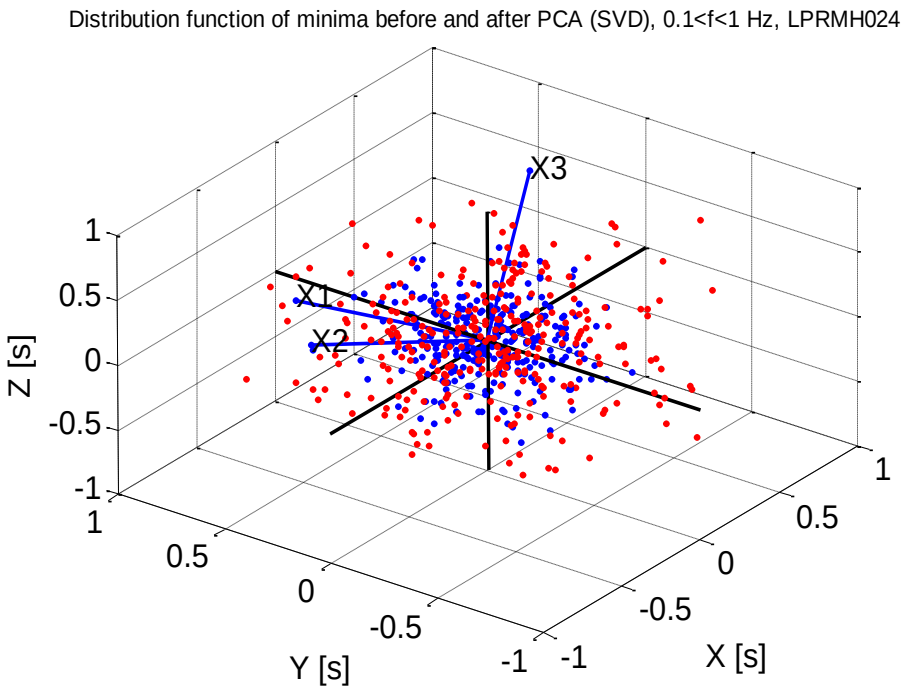

Fig. 35. Distribution of the vector points for LPRM 024 in operational point H, before (blue points) and after (red points) the application of PCA (SVD method).

4.5 Conclusions

This preliminary study served as kind of a warming up for the investigations of the applicability of some new methods for the stability analysis of BWRs. The goal was rather to get some acquaintance with the techniques applied, and to take into use some necessary steps (filtering and deriving the peak-to-peak time series) in order to apply the more advanced methods. These modest objectives were fulfilled and the potentials of the methods will be explored in further work. Among others the same method will be tried with a higher dimension of the data vectors formed from the peak-to-peak interval series.

Plans for the continuation

In stage 17 we plan to include the following parts in the current R&D program:

- Further development of the noise simulator, CoreSim, to be able to correctly model the noise induced by vibrating fuel assemblies, for the calculation of ex-core detector noise;
- Extension of the traditional Feynman-alpha and Rossi-alpha methods to two energy groups;
- Study of the dynamics of liquid fuel systems: extension of the model to two energy groups.

Acknowledgement

This project was supported by the Swedish Nuclear Power Inspectorate, contract No. SSM 2009/2093. Contact person was Assoc. Prof. Ninos Garis.

References

Bell G.I., Glassstone S., *Nuclear Reactor Theory*, Van Nostrand-Reinhold, New York, 1970.

Cacuci D.G., *On Chaotic Dynamics in Nuclear Engineering Systems*. Nucl. Technol., 103, pp. 303-309, 1993.

Cacuci D.G., March-Leuba J. and Perez R.B., *Limit Cycles and Bifurcations in Nuclear Systems*, Trans. Am. Nucl. Soc., 53, pp. 239, 1986.

D'Auria F. et al., *State of the Art Report on Boiling Water Reactor Stability – Appendix B: Methods for Evaluating Decay Ratio*. NEA report NEA/CSNI/R (96) 21, pp. 333-341, 1997.

Demazière C., *Development of a 2-D 2-group neutron noise simulator.* Annals of Nuclear Energy **19**, 647-680 (2004)

Demazière C. and Pázsit I., *On the possibility of the space dependence of the stability indicator (decay ratio) of a BWR*., Ann. Nucl. Energy 32, pp. 1305—1322, 2005.

Demazière C., Pázsit I., Sunde C. and Wright J., *Research and Development Program in Reactor Diagnostics and Monitoring with Neutron Noise Methods Stage 10. Final Report*, SKI report 04:57, 2004.

Demazière C. and Pázsit I., Power Reactor Noise, Lecture notes, Chalmers University of Technology, Göteborg, 2008.

Dulla, S. *Models and methods in the neutronics of fluid fuel reactors.* PhD These, Politecnico di Torino, March 2005

Dokhane A., *BWR Stability and Biffurcation Analysis using a Novel Reduced Order Model and the System Code RAMONA*, Ph.D. Thesis, EPFL, Switzeland, 2004.

Dykin, V and Pázsit I, *Remark on the role of the driving force in BWR instability*, Annals of Nuclear Energy **36**, 1544 – 1552, 2009

Dykin V., Demazière C, *Development of a Reduced Order Model and its application to the Forsmark-1 Instability Event of 1996/1997*, Internal report, CTH-NT-236, Chalmers University of Technology, Gothenburg, Sweden, August, 2010a.

Dykin, V, *The Effect of Different Perturbations on the Stability Analysis of Light Water Reactor,* Licentiate Thesis, CTH-NT-235, Chalmers University of Technology, Gothenburg, Sweden, September, 2010b.

Ginestar D., Miró R., Verdú G. and Hennig D., *A transient modal analysis of a BWR instability event. Journal of Nuclear Science and Technology* 39 (5), pp. 554– 563, 2002.

Ginestar D., Verdú G. and Miró R., *Singular system analysis of the local power range monitor (LPRM) readings of a boiling water reactor (BWR) in an unstable event*. International Jour-nal of Nuclear Energy Science and Technology 2 (3), pp. 253–265, 2006.

Hagen T.H.J.J. van der, Pázsit I., Thomson, O. and Melkerson B., *Methods for the determina-tion of the in-phase and out-of-phase stability characteristics of a boiling water reactor*. Nu-clear Technology 107 (2), pp. 193–214, 1994.

Hennig, D., *A study on boiling water reactor stability behaviour*. Nuclear Technology 126 (1), pp. 10–31, 1999.

Hotta A., Suzawa Y. and Takeuchi H., *Development of BWR regional instability model and verification based on Ringhals 1 test. Annals of Nuclear Energy* 24 (17), pp. 1403–1427,1997.

Karve A. A., *Nuclear-Coupled Thermal-hydraulic Stability Analysis of Boiling Water Reactors*, Ph.D. Thesis, Virginia University, USA, 1998.

Karlsson J. K-H. and Pázsit I., *Localisation of a channel instability in the Forsmark-1 boiling water reactor*. Ann. Nucl. Energy 26 (13), pp.1183-1204, 1999.

Konno H., Kanemoto S. and Takeuchi Y., *Parametric stochastic stability and decay ratio for a stochastic non-linear BWR model below the Hopf bifurcation*. Ann. Nucl. Energy 26, pp. 1465, 1999.

Kosály G. and Williams M.M.R., *Point theory of the neutron noise induced by inlet temperature fluctuations and random mechanical vibrations*, Atomkernenergie 18, pp. 203, 1971.

Kosály G., Meskó L., *Remarks on the transfer function relating inlet temperature fluctuations to neutron noise.*, Atomkernenergie 20, pp. 33—36, 1972.

Lahey T.R., *Boiling Heat Transfer. Modern Developments and Advances*, Elsevier Science Publishers, Amsterdam, London, New York, 1992

Lamarsh J. R., Introduction *to nuclear reactor theory*. American Nuclear Society, LaGrange Park, IL, USA, 2002.

Lange C.A., *Advanced Nonlinear Stability Analysis of Boiling Water Nuclear Reactors*, Ph.D. Thesis, Dresden Technical University", Germany, 2009.

MacPhee, J. *The Kinetics of Circulating Fuel Reactors.* Nucl. Sci. Engng 4, pp. 588-597, 1958.

March-Leuba J., Cacuci D.G. and Perez R.B., *Nonlinear Dynamics of Boiling Water Reactors*. Trans. Am. Nucl. Soc. 45, pp. 725, 1983.

March-Leuba J., Cacuci D.G. and Perez R.B., *Universality and Aperiodic Behavior of Nuclear Reactors*. Nucl. Sci. Eng., 86, pp. 401-404, 1984a.

March-Leuba J., *Dynamic behaviour of Boiling Water Reactors*, Ph.D. Thesis, University of Tennessee, USA, 1984b.

March-Leuba J., Cacuci D.G. and Perez R.B., *Nonlinear Dynamics and Stability of Boiling Wa-ter Reactors. I: Qualitative Analysis*. Nucl. Sci. Eng., 93, pp. 111-123, 1986a.

March-Leuba J., Cacuci D.G. and Perez R.B., *Nonlinear Dynamics and Stability of Boiling Wa-ter Reactors. II: Quantitative Analysis*. Nucl. Sci. Eng., 93, pp. 124-136, 1986b.

Morfill G. and Bunk W., *New designs on complex patterns.* Europhysics News, **32**, No. 3, 77 - 81 (2001)

Miró R., Ginestar D., Hennig D. and Verdú G., *On the regional oscillation phenomenon in BWRs*. Prog. Nucl. Energy 36 (2), pp. 189–229, 2000.

Munoz-Cobo J.L., Perez R. B., Ginestar D., Escriva A. and Verdu G., *Nonlinear Analisys of Out-of- Phase Oscillations in BWRs,* Annals of Nucl. Energy, 23, pp. 1301-1335, 1996.

Munoz-Cobo J.L., Chiva S. and Sekhri A., *A reduced order model of BWR dynamics with sub-cooled boiling and modal kinetics: application to out of phase oscillations*. Ann. Nucl. En-ergy 31 (10), pp. 1135-1162, 2004.

Oguma, R., *Application of noise analysis for the study of core local instability at Forsmark 1*. SKI report 97:42, Statens Kärnkraftinspektion (Swedish Nuclear Power Inspectorate), Stockholm, Sweden, 1997.

Pázsit I., *Neutron noise theory in the P_1 approximation*, Prog. Nucl. Energy 40, pp. 217—236, 2002.

Pázsit I., *Determination of reactor stability in case of dual oscillations.*, Ann. Nucl. Energy 22, pp. 378—387, 1995.

Pázsit I., Arzhanov V., Nordlund A. and Olsson D., *Research and Development Program in Reactor Diagnostics and Monitoring with Neutron Noise Methods Stage 9. Final Report*, SKI report 03:30, 2003 b

Pázsit I. and Demazière C., *Noise Techniques in Nuclear Systems*. In: Handbook of Nuclear Engineering, Ed. D. G. Cacuci, Springer, Chapter 14, Vol. 3, pp 1629-1737, 2010

Pázsit I., Demazière C. and Arzhanov V., *Research and Development Program in Reactor Diagnostics and Monitoring with Neutron Noise Methods Stage 8. Final report*, SKI report 03:08, 2003 a

Pázsit I., Demazière C., Arzhanov V. and Garis N. S., *Research and Development Program in Reactor Diagnostics and Monitoring with Neutron Noise Methods Stage 7. Final Report*, SKI report 01:27, 2001.

Pázsit I., Demazière C., Avdic S. and Dahl B., *Research and Development Program in Reactor Diagnostics and Monitoring with Neutron Noise Methods Stage 6. Final Report*, SKI report 00:28, 2000.

Pázsit I. and Garis N. S., *Forskningsprogram angående härddiagnostik med neutronbrusmetoder Etapp I. Slutrapport*, SKI report 95:14, 1995.

Pázsit I., Garis N. S., Karlsson J. and Rácz A., *Forskningsprogram angående härddiagnostik med neutronbrusmetoder Etapp 3. Slutrapport*, SKI report 97:31, 1997.

Pázsit I., Garis N. S. and Thomson O., *Forskningsprogram angående härddiagnostik med neutronbrusmetoder Etapp 2. Slutrapport*, SKI report 96:50, 1996.

Pázsit I. and Karlsson J K-H, *Research and Development Program in Reactor Diagnostics and Monitoring with Neutron Noise Methods Stage 4. Final report.*, SKI report 98:25, 1998.

Pázsit I., Karlsson J K-H, Lindén P. and Arjanov V., *Research and Development Program in Reactor Diagnostics and Monitoring with Neutron Noise Methods Stage 5. Final report*, 1999.

Pázsit I., Wihlstrand G., Tambouratzis T. and Dahl B., *Research and Development Program in Reactor Diagnostics and Moni.toring with Neutron Noise Methods, Stage 13,* SSM report 2008:39, 2008

Pázsit I., Wihlstrand G., Tambouratzis T., Jonsson A. and Dahl B., *Research and Development Program in Reactor Diagnostics and Monitoring with Neutron Noise Methods, Stages 14 and 15*, SSM report 2009:38, 2009.

Pázsit I. and Dykin V., *Investigation of the Space-Dependent Noise Induced by Propagating Perturbations.* Annals of Nuclear Energy **37**, 1329-1340, 2010

Sunde C., Pázsit I., Demazière C., Dahl B. and Mileshina L., *Research and Development Program in Reactor Diagnostics and Monitoring with Neutron Noise Methods Stage 11 and 12. Final report*, SKI report 2006:34, 2006

Takeuchi Y., Takigawa Y. and Uematsu H., *A study on boiling water reactor regional stability from the viewpoint of higher harmonics*. Nuclear Technology 106 (3), pp. 300–314, 1994.

Thie J. A., *Dynamic behavior of boiling reactors*. ANL-5849, Argonne National Laboratory, 1959.

Todreas N.E., Kazimi M.S., *Nuclear System I. Thermal-Hydraulic Fundamentals*, Hemisphere, New York, 1990.

Wach D. and Kosály G., *Investigation of the joint efrect of local and global driving sources in incore-neutron noise measurements.* , Atomkernenergie 23, pp. 244—250, 1974.

Wihlstrand, G. *The dynamics and noise diagnostics of molten salt reactor systems.* Chalmers internal report CTH-NT-222, October 2008

Yadigaroglu G. and Bergles A. E., *Fundamental and higher-mode density wave oscillations in two-phase flow*, Trans. ASME, C, J. Heat Transf. 94 (2), pp. 189–195, 1972.

Zinzani F., Demazière C. and Sunde C., *Calculation of the eigenfunctions of the two-group neutron diffusion equation and application to modal decomposition of BWR instabilities*. Annals of Nuclear Energy 35 (11), pp. 2109–2125, 2008.

2010:22

The Swedish Radiation Safety Authority has a comprehensive responsibility to ensure that society is safe from the effects of radiation. The Authority works to achieve radiation safety in a number of areas: nuclear power, medical care as well as commercial products and services. The Authority also works to achieve protection from natural radiation and to increase the level of radiation safety internationally.

The Swedish Radiation Safety Authority works proactively and preventively to protect people and the environment from the harmful effects of radiation, now and in the future. The Authority issues regulations and supervises compliance, while also supporting research, providing training and information, and issuing advice. Often, activities involving radiation require licences issued by the Authority. The Swedish Radiation Safety Authority maintains emergency preparedness around the clock with the aim of limiting the aftermath of radiation accidents and the unintentional spreading of radioactive substances. The Authority participates in international co-operation in order to promote radiation safety and finances projects aiming to raise the level of radiation safety in certain Eastern European countries.

The Authority reports to the Ministry of the Environment and has around 270 employees with competencies in the fields of engineering, natural and behavioural sciences, law, economics and communications. We have received quality, environmental and working environment certification.

Strålsäkerhetsmyndigheten
Swedish Radiation Safety Authority

SE-171 16 Stockholm
Solna strandväg 96

Tel: +46 8 799 40 00
Fax: +46 8 799 40 10

E-mail: registrator@ssm.se
Web: stralsakerhetsmyndigheten.se